

**REPORT DOCUMENTATION PAGE**

Public reporting burden for this collection of information is estimated to average 1 hour per response, including the time for reviewing instructions, searching existing data sources, gathering the required data, completing and reviewing this collection of information. Send comments regarding this burden estimate or any other aspect of this collection of information, including suggestions for reducing this burden, to Washington Headquarters Services, Directorate for Information Operations and Reports (0704-0188), 1215 Jefferson Davis Boulevard, Arlington, VA 22202-4302. Respondents should be aware that notwithstanding any other provision of law, no person shall be subject to any penalty for failing to comply with a collection of information if it does not display a currently valid OMB control number. PLEASE DO NOT RETURN YOUR FORM TO THE ABOVE ADDRESS.

0246

... if it does not display a currently

<b>1. REPORT DATE (DD-MM-YYYY)</b> 10-10-2003		<b>2. REPORT TYPE</b> Final Contractor Report		<b>3. DATES COVERED (From - To)</b> May 2001 - October 2003	
<b>4. TITLE AND SUBTITLE</b>  Calibration and Optimization of Constant Voltage Hot-Wire Anemometer in Hypersonic Flows				<b>5a. CONTRACT NUMBER</b> F49620-01-1-0244	
				<b>5b. GRANT NUMBER</b> N/A	
				<b>5c. PROGRAM ELEMENT NUMBER</b> N/A	
<b>6. AUTHOR(S)</b>  Chokani, Ndaona				<b>5d. PROJECT NUMBER</b> N/A	
				<b>5e. TASK NUMBER</b> N/A	
				<b>5f. WORK UNIT NUMBER</b> N/A	
<b>7. PERFORMING ORGANIZATION NAME(S) AND ADDRESS(ES)</b>  North Carolina State University Office of Contracts and Grants Campus Box 7214 Raleigh NC 27695-7214				<b>8. PERFORMING ORGANIZATION REPORT NUMBER</b> N/A	
<b>9. SPONSORING / MONITORING AGENCY NAME(S) AND ADDRESS(ES)</b> AFOSR/NA. Directorate: Aerospace and Materials Sciences Program: Unsteady Aerodynamics and Hypersonics 4015 Wilson Blvd. Arlington, VA 22203-1954				<b>10. SPONSOR/MONITOR'S ACRONYM(S)</b> AFOSR	
				<b>11. SPONSOR/MONITOR'S REPORT NUMBER(S)</b> N/A	
<b>12. DISTRIBUTION / AVAILABILITY STATEMENT</b> Approved for public release. Distribution unlimited.					
<b>13. SUPPLEMENTARY NOTES</b> N/A					
<b>14. ABSTRACT</b> Freestream and boundary layer measurements are made in a supersonic flow using both constant temperature (CTA) and constant voltage (CVA) anemometry. The performance of both anemometers is systematically made by operating the same hot-wire under identical conditions and applying post-test software corrections to the fluctuating measurements. In the case of the CVA the <i>in situ</i> time constant of the hot wire is measured to compensate the measured CVA output. The measurements show that when the signal-to-noise ratio is greater than one for both systems, the results are in very good agreement. The measurements of turbulence intensities are also in good agreement with previous studies. However the frequency at which noise dominates is lower for the CTA. Thus the CVA bandwidth is very much larger than that of the CTA. The amplitude roll-off at high frequencies is as theoretically expected. Thus it is desirable to obtain new quantitative turbulence measurements with larger bandwidth using the CVA. A rapid and automated stepping of the wire overheats is also developed for the CVA. This is an advancement over previous works that employed CTA, as the latter approach has a different bandwidth at each overheat, whereas the CVA has a fixed bandwidth. The rapid scanning method is then used to obtain calibrated measurements in a short duration wind tunnel.					
<b>15. SUBJECT TERMS</b> High-speed flows. Thermal Anemometry. Constant voltage anemometer.					
<b>16. SECURITY CLASSIFICATION OF:</b>			<b>17. LIMITATION OF ABSTRACT</b>  None	<b>18. NUMBER OF PAGES</b>  59	<b>19a. NAME OF RESPONSIBLE PERSON</b> Ndaona Chokani
<b>a. REPORT</b> Unclassified	<b>b. ABSTRACT</b> Unclassified	<b>c. THIS PAGE</b> Unclassified			<b>19b. TELEPHONE NUMBER (include area code)</b> 757-864-1103

20031104 009

**Table of Contents**

Acknowledgements	i
Nomenclature	ii
1.0 Introduction	1
2.0 Thermal Anemometry	4
2.1 Anemometer Approaches	5
3.0 Constant Voltage Anemometer	8
3.1 Constant Voltage Anemometer software correction	9
3.2 Constant Voltage Anemometer hot-wire time constant	10
3.3 Constant Voltage Anemometer – overheat of hot-wire	10
4.0 Experimental Apparatus	12
4.1 HMMS wind tunnel	12
4.2 Shock Wind Tunnel (SWK)	13
4.3 Constant Temperature Anemometer	13
4.4 Hot-wires	15
4.5 Data Acquisition System	15
5.0 Results and Discussion	17
5.1 HMMS Tunnel	17
5.2 Shock Wind Tunnel (SWK)	23
6.0 Concluding Remarks	26
7.0 References	28
8.0 Figures	33

**DISTRIBUTION STATEMENT A**  
Approved for Public Release  
Distribution Unlimited

## **Acknowledgements**

The partial support from the Air Force Office of Scientific Research under the grant F49620-01-0105 is gratefully acknowledged. The author is very greatly indebted to Dr. Garimella R. Sarma (Tao Systems) for many useful and extensive discussions concerning the constant voltage anemometer system. Joseph D. Norris (NC State) supported the data acquisition. The author also gratefully acknowledges the assistance of Helmut Knauss, Uwe Gaisbauer, Karl Heinz Laicher, Julien Weiss (Universität Stuttgart), Geneviève Comte-Bellot (Ecole Centrale de Lyon) and Alexander D. Kosinov (Russian Academy of Sciences – Siberian Branch) during the conduct of the experiments at Universität Stuttgart.

The views and conclusions contained herein are those of the author and should not be interpreted as necessarily representing the official policies or endorsements, either expressed or implied, of the Air Force Office of Scientific Research or the U.S. Government.

## Nomenclature

$a_w$	overheat ratio, $(R_w - R_{cold})/R_{cold}$
$A$	coefficient in hot-wire time constant equation derived from King's law
$b'$	amplification factor in the equation for CVA transfer function
$B$	coefficient in hot-wire time constant equation derived from King's law
$BW$	bandwidth of CVA
$c_p$	specific heat
$C$	capacitance in CVA circuit
$d$	wire diameter
$e'$	fluctuating voltage
$e_g'$	input perturbation for CTA electrical test
$E$	mean voltage
$f$	frequency
$f_s$	sampling frequency
$f_t$	gain bandwidth product of operational amplifier
$h'$	fluctuating wire heat transfer coefficient
$H$	mean wire heat transfer coefficient
$H_B(s)$	CTA transfer function to heat transfer input
$H_E(s)$	CTA transfer function to electrical input
$i'_w$	fluctuating wire current
$I_w$	mean wire current
$I_{offset}$	offset current in CTA circuit
$k_a$	thermal conductivity of air
$K$	amplifier gain in CTA circuit
$K_I$	constant
$m$	mass flux
$M_w$	hot-wire time constant
$P_w$	dissipated power in hot-wire
$r$	ratio of mass flux sensitivity and absolute value of total temperature sensitivity
$r'_w$	instantaneous wire resistance
	cable resistance
$r_L$	
$R_a, R_b, R_d$	resistances in CTA circuit
$R_A, R_B, R_D, R_I,$	resistances in CVA circuit
$R_F$	
$R_{cold}$	hot wire resistance at recovery temperature
$Re$	Reynolds number based on hot-wire diameter
$\mathcal{R}$	correlation coefficient
$s$	Laplace operator
$S$	sensitivity coefficient
$t$	time
$T_c$	hardware time constant

$T_m$	mass flux turbulence intensity
$T_o$	total temperature
$T_{To}$	total temperature turbulence intensity
$V_w$	wire voltage
$V_l$	voltage in CVA circuit
$x$	streamwise distance measured from nozzle throat
$y$	cross-stream distance measured from wind tunnel floor
$Z_b, Z_w$	impedances in CTA circuit

### Greek

$\delta$	boundary layer thickness
$\theta$	virtual total temperature fluctuation
$\rho$	density
$\omega$	frequency
$\omega_n$	natural frequency
$\zeta$	damping ratio

### Superscript

$\overline{\quad}$	mean value
--------------------	------------

### Subscripts

<i>cold</i>	condition of zero power dissipation
<i>i</i>	index
<i>L</i>	lead
<i>mean</i>	mean value
<i>rms</i>	root mean square value
<i>top</i>	top of CTA bridge
<i>u</i>	uncorrected
<i>w</i>	wire

### Abbreviations

CTA	constant temperature anemometer
CVA	constant voltage anemometer
IAG	Institut für Aerodynamik und Gasdynamik
ITAM	Institute of Theoretical and Applied Mechanics
PSD	power spectral density
SNR	signal-to-noise ratio
$\langle \rangle$	ratio of mean-square and square mean values

## **1.0 Introduction**

Air-breathing hypersonic flight vehicles are of interest to the Air Force in order to accomplish the goal of rapid global access. The occurrence of boundary layer transition affects the design of the airframe of air-breathing hypersonic flight vehicles, Reed *et al* (1997), because of its' direct impact on the flight vehicle's drag, the engine's performance and operability, and the requirements of the vehicle's thermal protection system. This is so as a turbulent boundary layer has higher skin-friction, higher surface heating and more mixing than a laminar boundary layer.

It is well known that boundary layer transition is a result of a sequential chain of processes, Reshotko (2001). The receptivity process transmits freestream disturbances into boundary layer instabilities. The resulting instabilities in a hypersonic boundary layer can include the first mode (Tollmien-Schlichting waves), crossflow vortices, Görtler vortices, and the second mode (Mack modes), Malik (1989). The freestream Mach number, surface geometry, surface temperature, and other parameters, modify the linear and nonlinear growth of the instabilities, their subsequent nonlinear interactions, and the eventual breakdown to turbulence. In hypersonic flows the linear amplification and nonlinear amplification & interactions are known to be the most critical processes in regards to the accurate prediction of transition, and of these processes the nonlinear stage is the most poorly understood, Chokani (1999), Kimmel and Kendall (1991).

The prediction of transition to turbulence in hypersonic flows is a difficult task. The state-of-the-art in transition prediction tools include PSE (Herbert, 1997; Chang, 2003) and DNS (Pruett and Chang, 1998) methods. PSE and DNS methods require a detailed knowledge of the freestream disturbance environment, which provides the necessary

forcing that generates the instability waves in the boundary layer (receptivity). The various stages in the evolution of the instabilities - linear growth, nonlinear growth, nonlinear saturation, and final breakdown – may then be simulated. The measurement of freestream disturbances is challenging as the experiments must be conducted in “quiet” hypersonic wind tunnels if an accurate representation of the flow physics is desired. The development of the quiet tunnel design technology is described by Beckwith *et al* (1983), Chen *et al* (1992, 1993) and Wilkinson (1997). The freestream disturbance levels in a “quiet” tunnel are one to two orders of magnitude less than those in conventional tunnels; these low levels are accomplished through the use of several design features in quiet tunnels. These features include boundary layer bleed slots just upstream of the nozzle throat, a highly polished nozzle surface and a well designed supersonic nozzle expansion section. Beckwith and Miller (1990) recommend that in a quiet tunnel, the static pressure fluctuations be less than 0.05%. Laufer (1961) suggests that the massflux fluctuations,  $m_{rms}/m_{mean}$  must be of the order of 0.1%. Therefore the measurement device must have high sensitivity.

In two-dimensional and axisymmetric hypersonic flows, the dominant boundary layer instability is the second mode. During the nonlinear stages, harmonics of the second mode are also significant. The frequency of the second mode disturbance is very closely given by  $U_e/(2\delta)$ , where  $U_e$ ,  $\delta$  are the boundary layer edge velocity and thickness, respectively. As the laminar boundary layers to be measured on test models in wind tunnels are thin, 2-3mm, the estimated frequency of the second mode disturbance is in the range 250kHz (Mach 5) to 700kHz (Mach 14). The frequency response requirement of

any measurement system in hypersonic flows is therefore quite demanding on account of the thin boundary layers and high velocities.

## 2.0 Thermal Anemometry

The most widely used device for measurements of amplitude and frequency fluctuations in hypersonic flows is the thermal anemometer, employing a hot-wire or hot-film sensor, Spina and McGinley (1994). Comprehensive reviews of the science of thermal anemometry are given by Bruun (1995) and Comte-Bellot (1998).

A hot-wire probe is a thin metallic element that is mounted between two broaches. It is practically possible to measure fluctuations up to 500kHz with hot-wires. A hot-film probe, which is a thin metallic film that is deposited onto a thick insulated substrate, has a bandwidth that is comparable to hot-wires. However, although they are more rugged than hot-wires, hot-film probes have poorer spatial resolution.

The sensor material has a temperature dependent resistance

$$R_w = R_{ref} [1 + \chi(T_w - T_{ref})]$$

Therefore the basic operating principle in thermal anemometry is to electrically heat the sensor, and then transduce into an output voltage the amount of heat transfer that occurs as fluid passes over the sensor. In a high-speed flow ( $M > 1.4$ ) the sensor simultaneously responds to both the mass flow and total temperature. This well-known mixed mode response of the sensor is generally given in the form presented by Morkovin (1956) as

$$\frac{e'}{e} = S_{\rho u} \frac{(\rho u)'}{(\rho u)} + S_{T_o} \frac{T_o'}{T_o}$$

Squaring and averaging yields

$$\frac{\overline{e'^2}}{\overline{e}^2} = S_{\rho u}^2 \frac{\overline{(\rho u)'^2}}{\overline{(\rho u)}^2} + 2S_{\rho u}S_{T_o} \frac{\overline{(\rho u)'T_o'}}{\overline{(\rho u)T_o}} + S_{T_o}^2 \frac{\overline{T_o'^2}}{\overline{T_o}^2}$$

The left-hand-side is known in terms of the mean and fluctuating outputs voltages. The sensitivity coefficients are known in terms of wire overheat. Thus the three unknowns on the right-hand-side, the normalized fluctuations of mass flux, the normalized correlation of mass flux-total temperature fluctuations and the normalized fluctuations of total temperature, can in principle be solved for using three overheats. However, in practice as there is scatter in experimental data, 10-12 overheats are used.

## **2.1 Anemometer Approaches**

The sensor can be operated under three different modes. Historically the first mode of operation is the constant current anemometer (CCA). The CCA, with full thermal lag compensation, has been used for high-speed fluctuation measurements.. Stetson et al (1983, 1984, 1985, 1989) and Kimmel (2001) used the CCA in hypersonic boundary layer stability experiments, which were conducted in the AEDC Tunnel B. More recently Corke et al (2002) used CCA to obtain measurements in the NASA Langley Research Center's Mach 3.5 quiet tunnel facility.

The second approach in thermal anemometry is the constant temperature (or resistance) mode. The practice of constant temperature anemometry (*CTA*) in high-speed flows is very well established, Smits et al (1983), Spina and McGinley (1994). The basic circuit for the *CTA* contains a Wheatstone bridge and an operational amplifier (op-amp). The op-amp provides a feedback current to the top of the bridge; if the sensor resistance varies during the operation of the *CTA*, this feedback restores the resistance to its original value. Therefore the feedback from the op-amp provides an automatic adjustment to the dynamic response of the hot-wire. However, several aspects of the *CTA* operation must be considered. The first is that the frequency response of the *CTA* depends upon the

overheat. Smits et al (1983) and Kegerise and Spina (2000) have observed that if the frequency response of a CTA is optimized at a high overheat, its bandwidth then decreases as the overheat is reduced. Since the hot-wire must be operated over a range of overheats for calibration and interpretation of the measured outputs in terms of mass flux and total temperature and the CTA bridge must first be adjusted before each measurement. It is not satisfactory to optimize the CTA bridge at a low overheat, as the bridge invariably becomes unstable at higher overheats. The second is that there is a change in the frequency response as the wire Reynolds number is changed, for example as the boundary layer is surveyed. Kegerise and Spina (2000) have observed that a CTA optimized at a high wire Reynolds number has a decrease in bandwidth as the wire Reynolds number is decreased. Conversely a CTA optimized at a low Reynolds number, can become unstable at higher Reynolds numbers. These two aspects whereby the frequency response of CTA depends upon the operating conditions (overheat and wire Reynolds number) mean that the CTA must be optimized at each measurement condition; therefore it may be a prohibitively time-consuming procedure to thoroughly document the evolution of disturbances through the linear and nonlinear regions of a hypersonic boundary layer. It is evident that CCA and CTA have some deficiencies with respect to bandwidth, sensitivity and signal-to-noise ratio. Indeed Lachowicz *et al* (1996) and Lachowicz and Chokani (1996) conducted the first systematic application using a CVA prototype in their quiet tunnel hypersonic boundary layer stability experiments. They observed that *"Only the CVA, in contrast to the attempts with the constant current and constant temperature anemometers, provided the ability to obtain measurable signals..."*. However at the time of the measurements the knowledge of constant voltage anemometer

was limited and thus only uncalibrated measurements were reported. The objective of the present work was therefore to verify the bandwidth, signal-to-noise and ease of operability of the constant voltage anemometer.

It is established theoretically, Sarma (1998) and experimentally, Kegerise and Spina (2000) that the CVA bandwidth does not change with overheat.

In the experiments conducted for the present work the bandwidth of the CVA (Tao Systems Model VC-01) was 470kHz. This bandwidth was determined by electrical injection of a sinewave signal using the setup shown in Figure 2. The measured bandwidth and phase responses are shown in Figure 3. Although the amplitude response is flat up to the stated bandwidth of 470kHz, it is evident that the phase response is flat to a lower frequency. This limited phase response may play a role in the interpretation of the results of high-order spectral analysis presented below. Note that the phase response is shifted by  $-90^\circ$  since no hot-wire is used in the electrical test and the pole associated with  $M_{CVA}$  is absent.

### 3.1 Constant voltage anemometer software correction

The transfer function of the CVA is given as

$$\frac{e'_{CVA,u}(s)}{u'(s)} = \frac{1 + T_c s}{1 + M_w^{CVA} s} \frac{I_w R_2 / R_w}{\left[ \left( \frac{s}{\omega_n} \right)^2 + \frac{1/T_c + 2\pi f_i R_w / R_d}{\omega_n^2} s + 1 \right]} b'$$

The hardware thermal compensation in the CVA is accomplished by the RC-network shown in Figure 1. The zero in the transfer function of the hardware time constant can be made to cancel the pole from the hot-wire time constant. However it is time consuming to always make this adjustment during tests as the hot-wire's time constant changes with overheat and wire Reynolds number, Comte-Bellot and Sarma (2001)

$$M_w^{CVA} = \frac{1 + a_w}{1 + 2a_w} \frac{d^2 \rho_w c_{p,w}}{4k_a} \frac{1}{A + B\sqrt{Re}}$$

Instead to retain the bandwidth that is associated with the fixed hardware time constant setting, a partial fixed hardware compensation in the CVA is used, and then corrected for with the measured *in situ* time constant of the hot-wire. The software correction applies the relation

$$e'_{CVA}(s) = e'_{CVA,u}(s) \left[ \frac{1 + M_w^{CVA} s}{1 + T_c s} \right]$$

in order to correct for the mismatch in the time constants. In the time domain the software correction is written as

$$e'_{CVA,i} = [e'_{CVA,u,i} (1 + M_w^{CVA} f_s) - f_s M_w^{CVA} e'_{CVA,u,i-1} + f_s T_c e'_{CVA,i-1}] (1 + T_c f_s)^{-1}$$

This sequence is initiated with the asymptotic result

$$e'_{CVA,i} = \frac{M_w^{CVA}}{T_c} e'_{CVA,u,i}$$

Therefore the approach of fluctuation measurements with partial fixed hardware compensation allows the CVA to be operated in a ‘free running’ mode without any of the time critical adjustments.

### 3.2 Constant voltage anemometer hot-wire time constant

In the experiments the *in-situ* hot-wire time constant is measured using the circuit shown in Figure 4. This circuit arrangement measures the first order CVA response to a 16Hz square wave that is injected through the resistance  $R_q$ . A 64 sample average CVA response is measured in the turbulent flows, and then the hot-wire time constant determined as the time taken to reach 63% of the final value.

### 3.3 Constant voltage anemometer – overheat of hot-wire

The hot-wire resistance is estimated from the measured  $E_{CVA}$  and  $V_w$  values using the CVA operating relation derived by applying Kirchoff’s current law

*Calibration and Optimization of Constant Voltage Hot-Wire Anemometer in Hypersonic Flows*

$$R_w = R_2 / [E_{CVA} / V_w - (1 + R_2 / R_F)] - r_L$$

Therefore the overheat of the hot-wire is given as  $a_w = (R_w - R_{cold}) / R_{cold}$ . For the CVA, the overheat is controlled by the user selected wire voltage,  $V_w$ . For work in short duration wind tunnels, manually changing  $V_w$  in order to obtain calibration measurements is prohibitive. An “automated stepping” system, which allows several wire voltages (and hence several overheats) to be set, was thus developed in the present work, Figure 5. This can be contrasted to the rapid scanning of multiple overheats using a CTA, which is problematic, Walker et al (1989), due to the coupled frequency response and overheat behavior in the CTA.

## 4.0 Experimental Apparatus

At the outset of the project the experiments to verify the bandwidth, signal-to-noise and ease of operability of the constant voltage anemometer were to be conducted in the NC State University supersonic wind tunnel. However due to building renovations the facility was unavailable. Instead the primary experiments were conducted in the half-model wind tunnel (German: **HalbModellMessStrecke**, HMMS) wind tunnel at Universität Stuttgart. This test opportunity also allowed subsequent tests to be performed in the Universität Stuttgart's shock wind tunnel (German: **StoßWindKanal**, SWK), as well as permitted direct *in-situ* comparisons to be made with a newly developed scanning CTA. Aside from the wind tunnels and anemometers, all the instrumentation and data acquisition systems that are used were purchased under this DURIP grant (F49620-01-1-0244).

### 4.1 HMMS wind tunnel

The primary experiment was conducted in the **HalbModellMessStrecke** (HMMS) wind tunnel at Universität Stuttgart. The HMMS is a suck-down supersonic wind tunnel, whose test section is bounded by one short expansion nozzle and the wind tunnel floor, Figure 6. The stagnation conditions are close to ambient conditions and the maximum run time of the tunnel is approximately 90secs. For the experiment, a Mach number 2.54 nozzle block is installed, and the measurements are performed on the boundary layer of the tunnel floor at one streamwise position,  $x=480mm$  downstream of the nozzle throat. Measurements with a Pitot tube and low constant current hot-wire show that at  $x=480mm$ , the boundary layer thickness is 7.5mm and the Reynolds number based on the momentum thickness is 4800. Analysis using the Harris-Blanchard boundary layer code shows that

transition occurs approximately 50mm downstream of the nozzle throat. Thus the boundary layer measured in the present experiment is not an equilibrium turbulent boundary layer; however, it is emphasized that in the present experiment the measurements are made in the same boundary layer flow using the same hot-wire with both CTA and CVA.

#### **4.2 Shock Wind Tunnel (SWK)**

The second experiments were conducted in the shock wind tunnel (German: StoßWindKanal, SWK) at Universität Stuttgart; the facility is described in Knauss *et al* (1999). The principle of the SWK operation is that of a shock tube with Laval nozzle. The tube diameter is 2.2m and the total length of the tunnel is 126m. The test section of SWK is 1.2×0.8m<sup>2</sup>, Figure 7, the test section Mach number is 2.54 and the flow duration is approximately 120ms. The unit Reynolds number is changed by varying the driver pressure. For the present work, six runs were performed; two runs each at a low, intermediate, and high Reynolds number. A total of 12 wire voltages were used, six in each run.

#### **4.3 Constant Temperature Anemometer**

The CTA used in the present study was built by the German company *Cosytec Elektronik GmbH*. Kosinov and Repkov (1998) designed the CTA circuit, Figure 8, for a high frequency response. It is a 1:10 bridge circuit, whose frequency response can be optimized using three parameters: the impedance in the passive arm of the bridge, the offset current (voltage), and the gain of the low noise, amplifier in the feedback loop. The resistance  $R_b$  in the passive arm of the bridge is used to vary the wire temperature (and

thus the overheat of the wire). More complete details of the CTA circuit are found in Weiss *et al* (2001).

The bandwidth of the CTA is not infinite but is limited by the ability of the feedback loop to provide automatic compensation. When optimized the bridge of the present CTA acts as a third-order low-pass filter with a cut-off frequency of about 100kHz. An electrical test is used to determine the actual frequency response of the CTA bridge and then correct the measured spectra. The procedure developed by Weiss *et al*(2001) is employed and yields CTA spectra that are accurate until the CTA's electronic noise is significant. For sake of completeness a few pertinent details of the procedure are repeated here. The desired bridge transfer function is

$$H_B(s) = \frac{e'_{CTA}(s)/E_{CTA}}{h'(s)/H}$$

In the electrical test, a 1kHz, square wave, voltage perturbation  $e'_g(s)$  is injected into the side of bridge at point A, Figure 8. The transfer function between the injected voltage and the CTA response is

$$H_E(s) = \frac{e'_{CTA}(s)}{e'_g(s)}$$

Since the transfer functions  $H_B(s)$  and  $H_E(s)$  have the same poles, but the transfer function of the electrical perturbations has an additional simple zero, whose time constant is close to that of the hot-wire's time constant,  $H_B(s)$  can then be written as

$$H_B(s) = K_1 \frac{s}{sM_w^{CTA} + 1} e'_{CTA}(s)$$

For the case where only frequencies greater than the thermal frequency of the wire are considered this equation can be approximated as

$$H_B(s) \approx K_1 \frac{1}{M_w^{CTA}} e'_{CTA}(s)$$

This measured frequency response of the bridge is then used in post-processing to correct the measured spectra of voltage fluctuations. An advantage of this correction approach is that an optimal bridge adjustment is not required for the CTA's fluctuation measurements; this enhances the test productivity.

#### 4.4 Hot-wires

The hot-wire used in the present tests is a tungsten wire of  $5\mu m$  diameter and  $1.2mm$  length. The hot-wire is spot-welded to the prongs of a commercial DANTEC® 55P11 probe. In the HMMS tunnel freestream the Reynolds number based on the wire diameter, and downstream normal shock conditions, is 25. The unit and wire Reynolds number for the six SWK runs are tabulated below.

**Reynolds numbers and overheats for the SWK runs.**

Run	Unit Reynolds Number $\times 10^6 / m$	Wire Reynolds Number $Re_w$	Overheat Ratio Range (six steps) $a_w$
1	2.50	12.5	0.07 - 0.73
2	2.28	11.4	0.78 - 1.44
3	4.53	22.6	0.05 - 0.55
4	4.63	23.1	0.53 - 1.02
5	6.49	32.4	0.05 - 0.48
6	6.46	32.3	0.49 - 0.91

#### 4.5 Data Acquisition System

For the HMMS tests, the CTA output voltage is AC-coupled at  $1kHz$  with a high-pass filter. The AC-coupled output voltage is then digitized, with 14-bit resolution, at  $800kHz$  using an IMTEC® A/D converter. The CTA itself has the characteristics of a low-pass  $100kHz$  3<sup>rd</sup> order elliptic filter. The CVA output voltage is AC-coupled and digitized

at  $2\text{MHz}$  using a Nicolet® Integra 40 digital storage oscilloscope having 12-bit resolution. The CVA unit itself incorporates the characteristics of a 6<sup>th</sup> order low pass Butterworth filter with a cut-off frequency of  $670\text{kHz}$ . No anti-aliasing filter is used with either anemometer unit.

For the SWK tests, the CVA output is acquired using the Nicolet® digital storage oscilloscope. The sampling frequency was  $2.5\text{MHz}$  and 500,000 samples were taken. The duration of each step of wire voltage is  $20\text{ms}$ , Figure 9.

## 5.0 Results and Discussion

### 5.1 HMMS Tunnel

The mean and rms anemometer output voltages are shown in Figure 10 for both measurement locations. The plot of the mean output voltages, Figure 10a, shows that, over the range of overheats examined, at a given measurement location the CVA values are 2-3 times the CTA values. The rms output voltages are shown in Figure 10b; for sake of clarity in the figure the values measured in the freestream are multiplied by a factor of 10. It is seen that at relatively low overheats the CTA values are greater than the CVA values; the converse is seen at relatively high values of the overheat. This behavior can be understood from an examination of the normalized hot-wire response

$$\frac{1}{S_{T_o}^2} \frac{\overline{e'^2}}{E^2} = \frac{a_w^2}{4} T_m^2 - a_w \Re T_m T_{T_o} + T_{T_o}^2$$

where the turbulence intensities and correlation coefficient are

$$T_m^2 = \frac{\overline{m'^2}}{\overline{m}^2}$$

$$\Re = \frac{\overline{m' T_o'}}{m_{rms} T_{o,rms}}$$

$$T_{T_o}^2 = \frac{\overline{T_o'^2}}{\overline{T_o}^2}$$

Comte-Bellot (1998) has derived expressions for the sensitivity coefficients for the CTA as

$$S_{m'}^{CTA} \approx \frac{1}{4}$$

$$S_{T_o}^{CTA} \approx -\frac{1}{2a_w}$$

Therefore the normalized CTA output is

$$\frac{\overline{e'^2}}{S_{T_o}^2 E^2} = 4a_w^2 \frac{\overline{e'^2}}{E^2}$$

For the CVA the sensitivity coefficients are

$$S_m^{CVA} \approx \frac{a_w}{2(1+2a_w)}$$

$$S_{T_o}^{CVA} \approx -\frac{1}{(1+2a_w)}$$

and the CVA's normalized output is

$$\frac{\overline{e^2}}{S_{T_o}^2 E^2} = (1+2a_w)^2 \frac{\overline{e^2}}{E^2}$$

If the output values at the top of CTA bridge are considered we get from the equality of the normalized anemometer outputs

$$\frac{\overline{e_{CVA}^2}}{e_{CTA_{top}}^2} = \frac{E_{CVA}^2}{E_{CTA_{top}}^2} \frac{4a_w^2}{(1+2a_w)^2}$$

The voltage at the top of the CTA bridge can be determined from the measured wire voltage. The result for both measurement locations is shown in Figure 11. This shows an equality of the rms output voltages when  $a_w \approx 0.54$ . This corresponds well with the result shown in Figure 10. The ratio of the mean square (that is, variance) and square mean output voltages is shown in Figure 12. Over the range of overheats test the CTA values are in excess of the CVA values. However whereas the CVA values show little variation with overheat, the CTA values increase dramatically at low overheats; this feature is characteristic of the well known nonlinear CTA response to total temperature at low overheats, Smits et al (1983).

The post-test software correction applied to both the CTA and CVA fluctuation measurements is examined Figures 13-16. The spectra of the fluctuating CTA output voltage, measured in the freestream, Figure 13, for three overheats,  $a_w = 0.22, 0.63$  and  $1.05$  and in the boundary layer at  $y/\delta = 0.36$ , Figure 14, for  $a_w = 0.21, 0.60$  and  $1.01$  are shown. The shape of the CTA spectra are quite different with and without the correction.

The uncorrected spectra show a sharp decrease in amplitude above the cut-off frequency. On the otherhand the corrected spectra show the characteristic  $f^2$  rise due to electrical noise once the SNR is less than one, Freymuth (1968), Saddoughi and Veeravali (1996). For the freestream measurements this rise starts at  $f \approx 30\text{kHz}$ . In the boundary layer the  $f^2$  rise starts at  $f = 200\text{kHz}$ . In the freestream where the turbulence levels are relatively low, at the two higher overheats the SNR becomes less than unity below the cut-off frequency whereas its becomes less than unity above the cut-off frequency at the lower overheat. Thus the  $f^2$  rise is not seen in the uncorrected CTA spectra at the low overheat. The effect of strain gauging in the hot-wire is quite apparent in the spectra measured in the boundary layer. Thus while the software correction is quite effective in correcting the data to above the cut-off frequency, the SNR is less than unity only at around  $200\text{kHz}$ , the strain gauging limited the usefulness of some of the higher frequency data. In the present study, the rms voltages, for both CTA and CVA, are determined in the frequency range  $1\text{--}20\text{kHz}$  for the freestream and  $1\text{--}100\text{kHz}$  for the boundary layer. A comparison of the uncorrected CTA spectra shows that the cut-off frequency decreases dramatically with decreasing overheat. On the otherhand the corrected CTA spectra show a much smaller change in the cut-off frequency as the overheat is changed.

The spectra of the fluctuating CVA output voltage for the corresponding overheats are presented in Figures 15 and 16. The uncorrected and corrected CVA spectra show the same qualitative characteristics in both the freestream and boundary layer. Quantitatively the uncorrected and corrected CVA spectra differ only in their levels. In comparison with the CTA this unchanged characteristic may be advantageous in providing a preliminary evaluation of test data during actual wind tunnel testing. In the freestream, the SNR is

seen to become less than one at a frequency of approximately  $50\text{kHz}$ . In the boundary layer the SNR is greater than unity up to the measured bandwidth of  $470\text{kHz}$ . The effect of wire strain gauging is also observed in the CVA spectra, suggesting that this phenomenon is not anemometer dependent. At both measurement locations the effective bandwidth for the CVA is seen to be larger than the CTA spectra, and this bandwidth does not change with overheat. In contrast to the CTA spectra, the CVA spectra show little sensitivity of the bandwidth as the overheat is changed.

The corrected CTA and CVA spectra are directly compared in Figures 17 and 18. The importance of the transfer function correction for the CTA is seen, as the general features of the CTA spectra are in good agreement with the CVA spectra. At both measurement stations, as was previously suggested, it is seen that at low overheats the spectral levels from the CTA are greater than from the CVA; the converse is seen at the higher overheats. At the intermediate overheat the spectral levels of the two anemometers are comparable over the frequency range where  $\text{SNR} > 1$ . In the freestream, it is quite evident that the noise rise in the CTA spectra occurs at a lower frequency than the CVA. As the hot-wire is operated under identical conditions, this clearly indicates that the CVA is superior to the CTA in terms of SNR. The better SNR characteristics of the CVA are again evident in the boundary layer where the turbulence levels are much higher than in the freestream. For the CTA the SNR is greater than unity up to a frequency of  $300\text{kHz}$ ; on the otherhand the CVA provides useful measurements up to its' measured bandwidth of  $470\text{kHz}$ . However as discussed above for both anemometers there is strain gauging of the hot-wire, which limits our ability to provide quantitative comparisons above  $200\text{kHz}$ .

**Turbulence intensities and correlation coefficient**

$y/\delta$		$T_m$ , %	$\mathcal{R}$	$T_{To}$ , %
1.5	CTA	0.32	-0.01	0.06
	CVA	0.39	0.38	0.09
0.36	CTA	13.0	0.36	2.0
	CVA	14.0	0.43	1.8

The turbulence intensities and correlation coefficient can be computed using

$$\frac{1}{S_{T_o}^2} \frac{\overline{e'^2}}{E^2} = \frac{a_w^2}{4} T_m^2 - a_w \mathcal{R} T_m T_{T_o} + T_{T_o}^2$$

The frequency ranges used to compute these data are 1-20kHz in the freestream and in the boundary layer 1-100kHz. The turbulence levels,  $T_m$ ,  $T_{To}$ , in the freestream are typical of those that are obtained in conventional high-speed wind tunnels. The agreement between the two anemometers is good. However the correlation coefficient between the CTA and CVA differ significantly; this difference is surprisingly large and is indicative of the sensitivity of the correlation coefficient to the curve-fit procedure. The turbulence levels and correlation coefficient measured in the boundary layer with the two anemometers are in very good agreement with each other and are also comparable to those of Kistler (1959) Smits *et al* (1983) Sarma *et al* (1998) and Comte-Bellot and Sarma (2001) amongst others; however we should again note that in the present experiment there is not an equilibrium turbulent boundary layer.

The classical form of the fluctuation diagram,

$$\Theta^2 = T_m^2 r^2 - 2\mathcal{R}r + T_{T_o}^2$$

where

$$\Theta = \frac{e'}{S_{T_o} E} \quad \text{and} \quad r = \frac{S_m}{|S_{T_o}|} = \frac{a_w}{2}$$

is shown in Figure 19. Theoretically the results for both anemometers should be identical. However differences are seen, most significantly at low overheats. The CVA and CTA values are in good agreement for  $r \geq 0.15$ , in the freestream measurements, and  $0.07 \leq r \leq 0.45$  in the boundary layer measurements. However at the lower overheats in the freestream the CVA values are greater than the CTA values. A similar behavior was observed by Bestion et al (1983) in their comparison of CCA and CTA; however to the author's knowledge, to-date, no direction comparison of the fluctuation diagrams of CCA and CVA has been made. Bestion et al (1983) attribute this difference to the nonlinear response of the CTA to total temperature at low overheats. A comparison of the CCA and CVA in this regard may resolve the source of this discrepancy.

The mass flux and total temperature power spectra are shown in Figures 20 and 21.

These spectra are obtained by fitting a second order curve to  $PSD_{<e^2>}$  vs.  $r$  since

$$PSD_{\{e^2\}} = S_m^2 PSD_{\{m^2\}} + 2S_m S_{T_o} PSD_{\{mT_o\}} + S_{T_o}^2 PSD_{\{T_o^2\}}$$

and then evaluating the massflux and total temperature power spectral densities from the coefficients; this curve-fitting procedure does invariably introduce some scatter in the mass flux and total temperature power spectra. In the freestream, Figure 20, the CTA spectral levels are somewhat lower than the CVA levels. In the boundary layer, Figure 21, the abscissa is plot with  $f^{5/3} \times PSD$  as there is a decay of  $-5/3$ ; the measured slope at high frequencies is  $-1.44$ , which compares very well with the expected decay. Overall the agreement between the CTA and CVA is excellent. As can be clearly seen this slope

in the CVA spectra continues up to its bandwidth of 470kHz. This confirms the utility of the CVA for providing the large bandwidth measurements that are desired for the study of compressible transition and turbulence.

## 5.2 SWK Tunnel

In the present work the application of the CVA in a short run time supersonic wind tunnel facility was also developed. In addition to automating the acquisition of hot-wire measurements at multiple overheats for calibrated data, this is highly desirable as, in the relatively short run times of high-speed facilities, these multiple overheats within a single run assure accuracy in the measured data.

It is usual practice to measure the hot-wire time constant at the hot-wire's operating point. However, in a short duration wind tunnel a difficulty arises as it is not possible to experimentally measure the hot-wire time constant,  $M_{CVA}$ . This difficulty arises since the time averaged hot-wire response to an electronically injected 20Hz square wave is used to obtain the hot-wire time constant  $M_{CVA}$ . Since a frequency of 20Hz corresponds to a 50ms time period, this time period cannot provide any averages over the 20ms interval of each constant wire voltage step, Figure 9. For the present experiments, which are performed in the shock wind tunnel, the hot-wire time constant was thus estimated using

$$M_w^{CVA} = \frac{1 + a_w}{1 + 2a_w} \frac{d^2 \rho_w c_{p,w}}{4k_a} \frac{1}{A + B\sqrt{Re}}$$

and the measured wire Reynolds numbers and overheat ratios. The estimated hot-wire time constants are plotted versus overheat for the runs conducted in SWK, Figure 22.

The spectra are presented in Figure 23 for the both the raw and corrected CVA output voltage for low and high overheat values at a low, intermediate, and high unit Reynolds numbers. As observed above, the thermal lag software correction increases all

of the spectral levels but does not change the shape of the spectra. The comparison of the low Reynolds number spectra, Figures 23a and 23b, shows that the level of the PSD increases as the overheat ratio increases. A similar trend is seen when comparing the intermediate Reynolds numbers and high Reynolds numbers spectra. It should be noted that the high frequency sharp peaks are a result of strain gauge effects on the hot-wire.

In all of the spectra, a rise is seen to occur at frequencies greater than  $20\text{kHz}$ . This rise is due to the electronic noise exceeding the levels of measurable signals in that frequency range. Thus, only the spectral levels in the frequency range  $1\text{kHz} \leq f \leq 20\text{kHz}$  are of physical significance.

It is known that a hot-wire in a supersonic flow has a mixed mode response to both mass flux and total temperature fluctuations. At low overheats the hot-wire is primarily responsive to total temperature and at high overheats to mass flux. The spectra at low overheat are relatively flat and qualitatively indicate that the total temperature fluctuations are small. At high overheats, the spectral levels in the significant frequency range are elevated. As expected, the levels in these spectra decrease with increasing frequency indicating that the mass flux fluctuations are more pronounced.

#### Normalized RMS fluctuations and correlation coefficient in SWK.

$Re_w$	$T_{\rho u}$ [%]	$R$ [%]	$T_{T_0}$ [%]
12.5, 11.4	$2.0887 \times 10^{-1}$	$6.5789 \times 10^{-5}$	$6.2958 \times 10^{-2}$
22.6, 23.1	$3.8848 \times 10^{-1}$	$-2.5238 \times 10^{-5}$	$5.6144 \times 10^{-2}$
32.4, 32.3	$2.4004 \times 10^{-1}$	$-3.0159 \times 10^{-5}$	$4.0747 \times 10^{-2}$

Fluctuation diagrams are presented in order to characterize the different modes that may be present in a supersonic freestream flow. Kovasznay (1953) described the three

significant modes in a supersonic flow as vorticity, entropy, and sound-wave modes. The vorticity mode is synonymous with turbulence, the entropy mode is described as “temperature spottiness”, and the sound-wave mode are the acoustic disturbances within the flow field.

Figure 24 shows the measured fluctuation diagrams for the three sets of Reynolds numbers. In each diagram the solid line is derived from the equation  $\Theta^2 = T_m^2 r^2 - 2\Re + T_e^2$  using the turbulence levels and correlation coefficient presented in the above Table. It can be seen that the normalized RMS mass flux fluctuations are an order of magnitude larger than the normalized RMS total temperature fluctuations as is suggested from the spectra presented above. Overall, the results show that the SWK tunnel has very low levels of freestream fluctuations. The overheat ratio, and variance and mean values of the CVA output are experimentally measured. The variance is obtained by performing a “band limited” integration of the spectrum over the frequency range  $1kHz < f < 20kHz$ . Each diagram shows a decrease in slope or inflection at low values of  $r$ ; this indicates the contribution of the vorticity mode to the freestream fluctuations. In none of the diagrams does the asymptotic straight line indicate an intercept with the origin. Thus temperature spottiness contributes to the fluctuations in SWK; this is possible since the majority of the tunnel lies outdoors and is therefore susceptible to nonuniform solar heating. As may be expected with a supersonic wind tunnel, the acoustic mode is the most dominant.

## **6.0 Concluding Remarks**

The bandwidth, signal-to-noise and ease of operability of the constant voltage anemometer is assessed. This is accomplished by making a systematic comparison of the performance of CTA and CVA in supersonic flows. In the present experiments the same hot-wire was operated at the same locations under the same conditions with both systems. A post-test software correction is applied to the fluctuation measurements in both systems. For the CTA the bridge's frequency response is obtained at each wire temperature; this is then used to correct the measured data for the changes in the bridge's dynamic behavior as the wire temperature is changed. In the case of the CVA the in situ time constant of the hot-wire is measured at each wire temperature; the measured time constant are then applied to the fixed compensation output of the CVA.

The software correction in the CVA makes no qualitative change to the character of the spectra; however the spectral levels are adjusted by a factor close to the square of the ratio of the hot-wire and hardware compensation time constants. In the CTA the character of the spectra are qualitatively and quantitatively different, in particular above the cut-off frequency. As the cut-off frequency is independent of the signal-to-noise ratio, it is necessary to apply a correction for the bridge response if accurate CTA measurements are desired.

The software corrected CTA and software corrected CVA spectra are in very good agreement when the signal-to-noise ratio is above unity. For low overheats, less than 0.6 for the present CTA, the levels in the power spectra of CTA output voltages are greater than those of the CVA output voltages. For higher overheats the levels in the power spectra of CVA are greater than in the CTA. This relative change in the output levels is

an expected behavior. However the frequency at which noise dominates is lower for the CTA (higher for the CVA). Thus the CVA bandwidth is very much larger than that of the CTA.

The turbulence measurements, fluctuation diagrams, and spectra of massflux and total temperature are also examined. The turbulence levels for both CTA and CVA show relatively good agreement with previous measurements. The fluctuation diagrams show good agreement at moderate to high overheats; however at low overheats the difference is attributed to the nonlinear behavior of the CTA. The spectra of massflux and total temperature are in good agreement in the frequency range where the signal-to-noise ratio is above unity. The amplitude roll-off at high frequencies is in good agreement with theory.

The rapid and automated adjustment of the wire voltage of CVA system was developed and demonstrated.. This capability is demonstrated in the measurement conducted in a short duration supersonic wind tunnel. The turbulent intensities are measured and the power spectral densities are derived. The results indicate that the tunnel has relatively low levels of freestream disturbances that are confined to frequencies less than 10kHz. Fluctuation diagram analysis shows that characteristics of the disturbances are acoustic and vortical in nature. This new capability enhances the ability to obtain calibrated data in future hypersonic boundary layer stability experiments.

## 7.0 References

1. Beckwith, I. E., Creel Jr., T. R., Chen, F.-J., and Kendall, J. M., "Freestream noise and transition measurements on a cone in a Mach 3.5 pilot low-disturbance tunnel," *NASA TP 2180* (1983).
2. Beckwith, I. E. and Miller, C. G., "Aero-thermodynamics and transition in high-speed wind tunnels at NASA Langley," *Annu. Rev. Fluid Mech.*, **22**, 419 (1990).
3. Bestion, D., Gaviglio, J. and Bonnet, J. P., "Comparison Between Constant-Current and Constant-Temperature Hot-Wire Anemometers in High-Speed Flows," *Rev. Sci. Instrum.*, Vol. **54**, 1513 (1983).
4. Bruun, H. H., "*Hot-Wire Anemometry, Principle and Physical Analysis*," Oxford Science, New York, 1995.
5. Bushnell, D. M., Applications and Suggested Directions of Transition Research," *Proc. Fourth Symposium on Numerical and Physical Aspects of Aerodynamic Flows*, January 1989.
6. Chang, C.-L., "The Langley Stability and Transition Analysis Codes (LASTRAC: LST, linear and nonlinear PSE for 2D, axisymmetric, and infinite swept wing boundary layers," *AIAA 2003-0974* (2003).
7. Chen F.-J., Malik, M. R. and Beckwith, I. E., "Görtler instability and supersonic quiet nozzle design," *AIAA J.*, **30**, 2093 (1992).
8. Chen, F.-J., Wilkinson, S. P., and Beckwith, I. E., "Görtler instability and hypersonic quiet nozzle design," *J. Spacecraft & Rockets*, **30**, 170 (1993).
9. Chokani, N., "Nonlinear spectral dynamics of hypersonic laminar boundary layer flow," *Phys. Fluids*, **11**, 3846 (1999).

10. Comte-Bellot, G., “*Hot-Wire Anemometry*,” Handbook of Fluid Dynamics, (Johnson, R. W. Ed.), CRC Press, Boca Raton FL, 1998, Chap. 34.
11. Comte-Bellot, G. and Sarma, G. R., “Constant voltage anemometer practice in supersonic flows,” *AIAA J.*, **39**, 261 (2001).
12. Corke, T. C., Cavalieri, D. A., Matlis, E., “Boundary-layer instability on sharp cone at Mach 3.5 with controlled input,” *AIAA J.*, **40**, 1015 (2002).
13. Freymuth, P., “Noise in hot-wire anemometers,” *Rev. Sci. Instrum.*, **4**, 550 (1968).
14. Herbert, T., “Parabolized stability equations,” *Annu. Rev. Fluid Mech.*, **29**, 245 (1997).
15. Horvath, T. J., Berry, S. A., Hollis, B. R., Chang, C.-L., and Singer, B. A., “Boundary layer transition on slender cones in conventional and low disturbance Mach 6 wind tunnels,” *AIAA 2002-2743* (2002).
16. Kegerise, M. A. and Spina, E. F., “A comparative study of constant-voltage and constant-temperature hot-wire anemometers: part ii – the dynamic response,” *Expts. Fluids*, **29**, 165 (2000).
17. Kimmel, R. L., “Hypersonic Boundary Layer Stability Measurements using Uncalibrated Hot Wires,” *AIAA 2001-0275*, (2001).
18. Kimmel, R. L. and Kendall, J. M., “Nonlinear disturbances in a hypersonic boundary layer,” *AIAA 91-0320*, (1991).
19. Knauss, H., Riedel, R. and Wagner, S., “The shock wind tunnel of Stuttgart University: a facility for testing hypersonic vehicles,” *AIAA 99-4959*, (1999).

20. Kosinov, A. D. and Repkov, V. V., "Design and application of CTA in supersonic flow," *Proceedings of the International Conference on the Methods of Aerophysical Research*, (1998).
21. Lachowicz, J. T., Wilkinson, S. P., and Chokani, N., "Hypersonic boundary layer stability over a flared cone in a quiet tunnel," *AIAA J.*, **34**, 2496 (1996).
22. Lachowicz, J. T., and Chokani, N., "Hypersonic boundary layer stability experiments in a quiet tunnel with bluntness effects," *NASA CR 198272* (1996).
23. Laufer, J., "Aerodynamic Noise in Supersonic Wind Tunnels," *J. Aeronaut. Sci.*, **28**, 685 (1961).
24. Malik, M. R., "Prediction and control of transition in supersonic and hypersonic boundary layers," *AIAA J.*, **27**, 1487 (1989).
25. Morkovin, M. V., "Fluctuations and hot-wire anemometry in compressible flows," *AGARDograph 24*, (1956).
26. Pruett, C. D., and Chang, C.-L., "Direct numerical simulation of hypersonic boundary-layer flow on a flared-cone," *Theoret. Comput. Fluid Dynamics*, **11**, 49 (1998).
27. Reed, H. L., Kimmel, R., Schneider, S. P., and Arnal, D., "Drag prediction and transition in hypersonic flow," *AIAA 97-1818* (1997).
28. Reshotko, E., "Transient growth: a factor in bypass transition," *Phys. Fluids*, **13**, 1067 (2001).
29. Saddoughi, S. G. and Veeravali, S. V., "Hot-Wire Anemometry Behavior at Very High Frequencies," *Meas. Sci. Tech.*, **7**, 1297 (1996).

30. Sarma, G. R. "Transfer Function Analysis of the Constant Voltage Anemometer"  
*Rev. Sci. Instrum.*, **69**, 2385 (1998).
31. Sarma, G. R., Comte-Bellot, G. and Faure, T. M., "Software Corrected Hot Wire Thermal Lag for the Constant Voltage Anemometer Featuring a Constant Bandwidth at the Selected Compensation Setting," *Rev. Sci. Instrum*, **69**, 3223 (1998).
32. Smits, A. J., Hayakawa, K. and Muck, K. C., "Constant-temperature hot-wire anemometer practice in supersonic flows- part 1- the normal wire," *Expts. Fluids*, **1**, 83 (1983).
33. Spina, E. F., and McGinley, C. B., "Constant-temperature anemometry in hypersonic flow: critical issues and sample results," *Expts. Fluids*, **17**, 365 (1994).
34. Stetson, K. F., Thompson, E. R., Donaldson, J. C., and Siler, L. G., "Laminar boundary layer stability experiments on a cone at Mach 8, part 1: sharp cone," *ALAA* 83-1761 (1983).
35. Stetson, K. F., Thompson, E. R., Donaldson, J. C., and Siler, L. G., "Laminar boundary layer stability experiments on a cone at Mach 8, part 2: blunt cone," *ALAA* 84-0006 (1984).
36. Stetson, K. F., Thompson, E. R., Donaldson, J. C., and Siler, L. G., "Laminar boundary layer stability experiments on a cone at Mach 8, part 3: sharp cone at angle of attack," *ALAA* 85-0492 (1985).
37. Stetson, K. F., Thompson, E. R., Donaldson, J. C., and Siler, L. G., "Laminar boundary layer stability experiments on a cone at Mach 8, part 5: tests with a cooled model," *ALAA* 89-1895 (1989).

38. Walker, D. A., Ng, W. F., and Walker, M. D., "Experimental comparison of the two hot-wire techniques in supersonic flow," *AIJA J.*, **27**, 1074 (1989).
39. Weiss, J., Knauss, H., Wagner, S. and Kosinov, A. D., "Constant temperature hot-wire measurements in a short duration supersonic wind tunnel," *Aeronautical Journal*, 435 (2001).
40. Wilkinson, S. P., "A review of hypersonic boundary layer stability experiments in a quiet Mach 6 wind tunnel," *AIJA 97-1819* (1997).

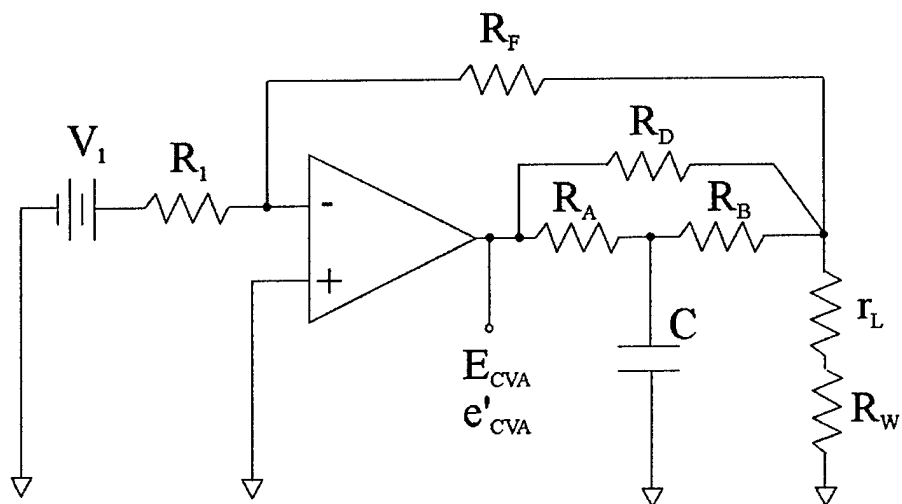


Figure 1: CVA circuit.

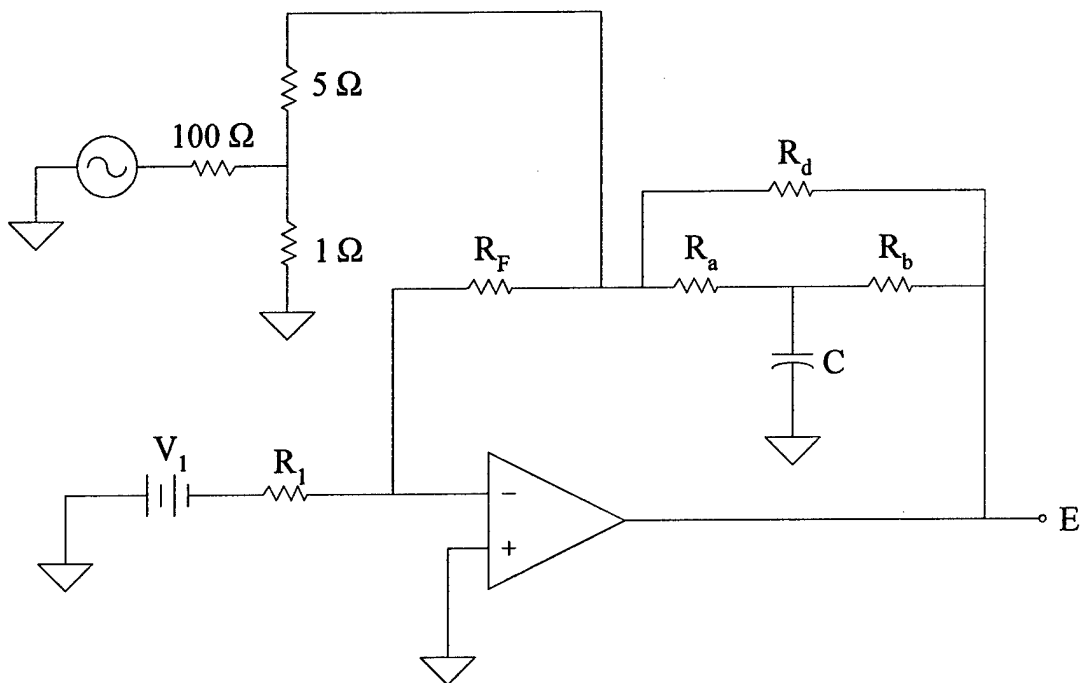
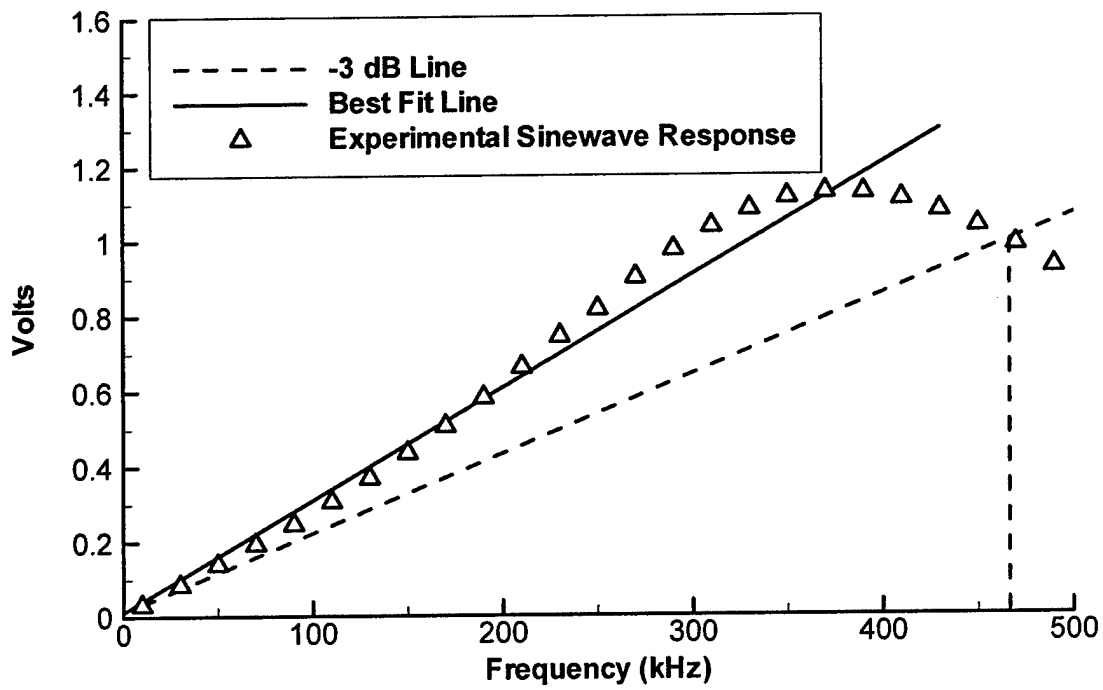
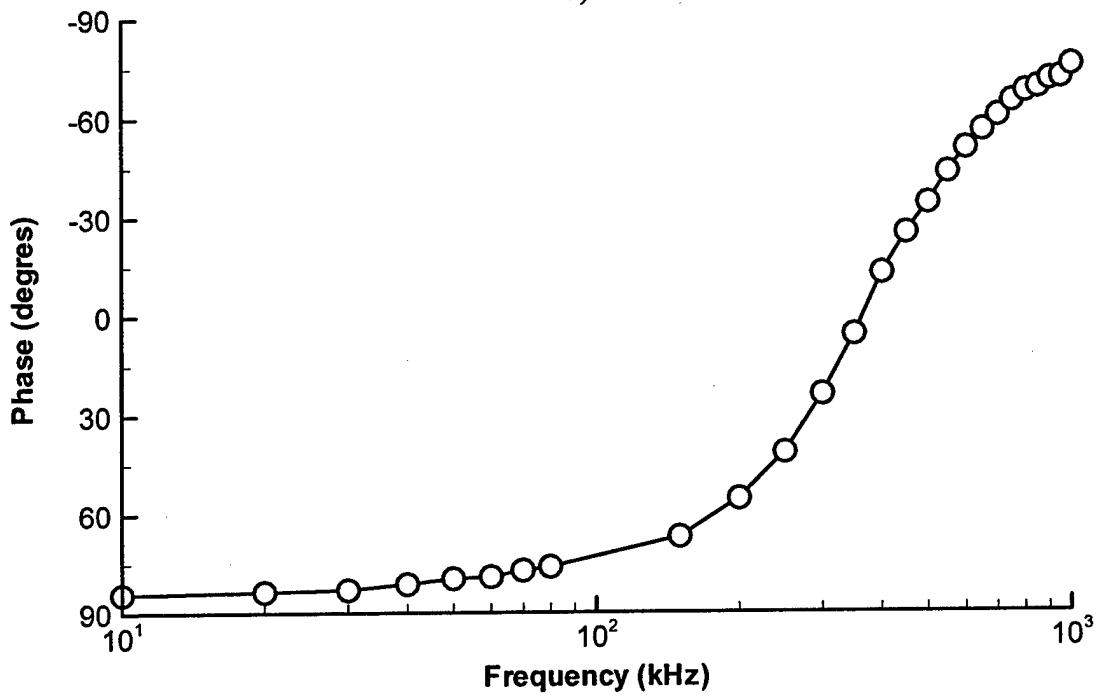


Figure 2: Sinewave test setup for bandwidth determination



a)



b)

Figure 3: a) Amplitude and b) phase response of CVA determined by sinewave injection.

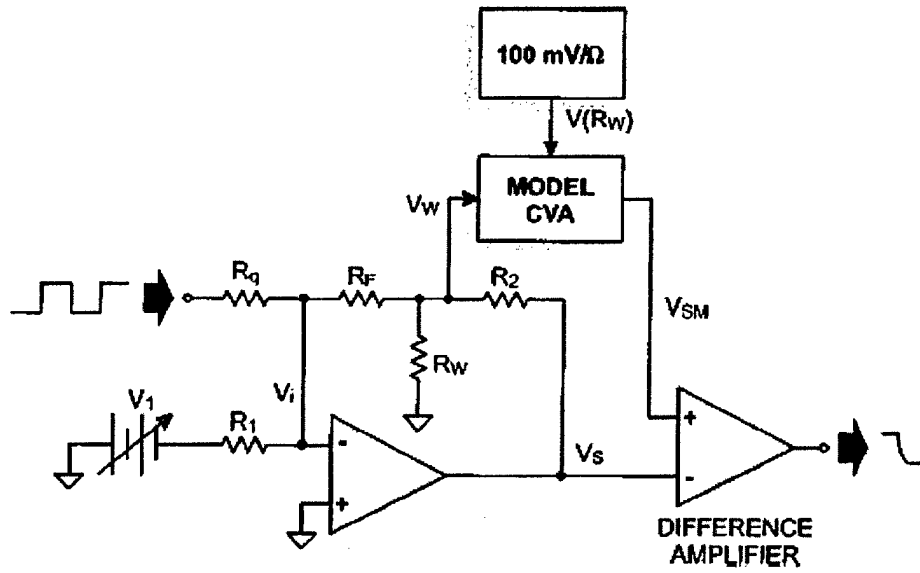
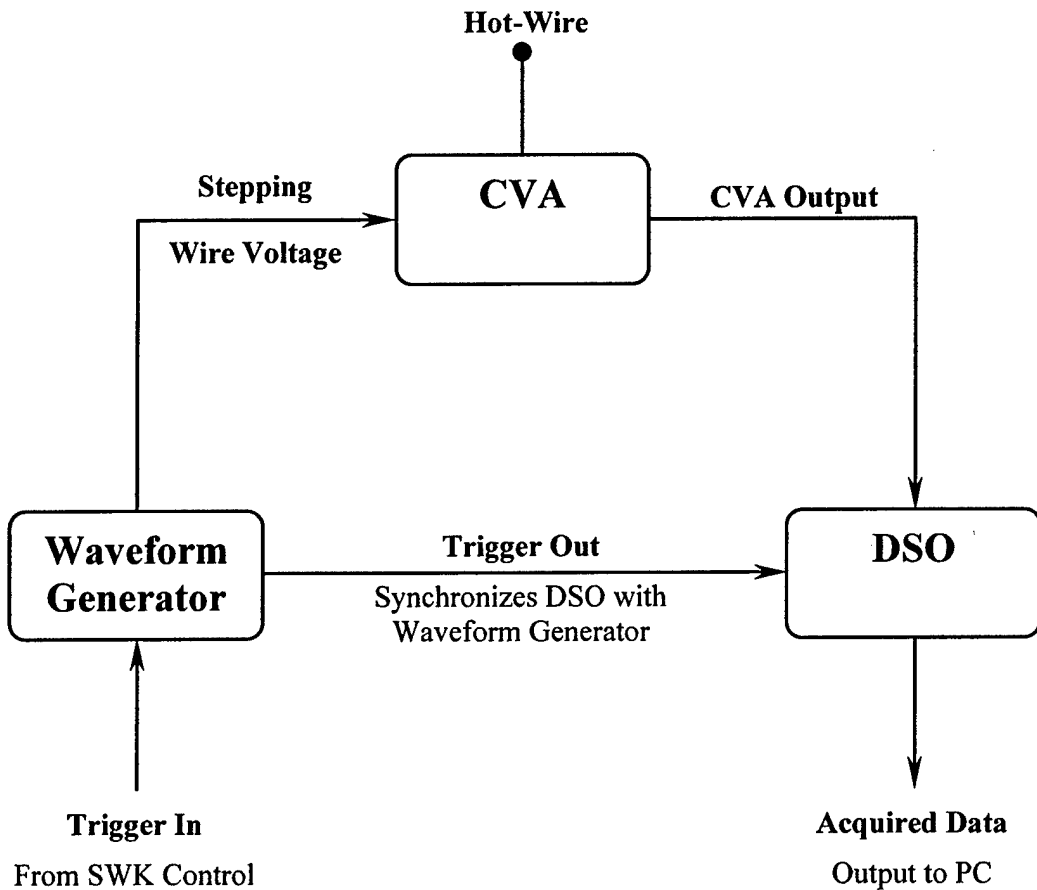


Figure 4: CVA circuit for determination of hot-wire time constant.



**Figure 5: Block diagram of the instrumentation set-up for the “automatic stepping” experiments.**



*Calibration and Optimization of Constant Voltage Hot-Wire Anemometer in Hypersonic Flows*

Figure 6: Test section of the HalbModellMessStrecke (HMMS).

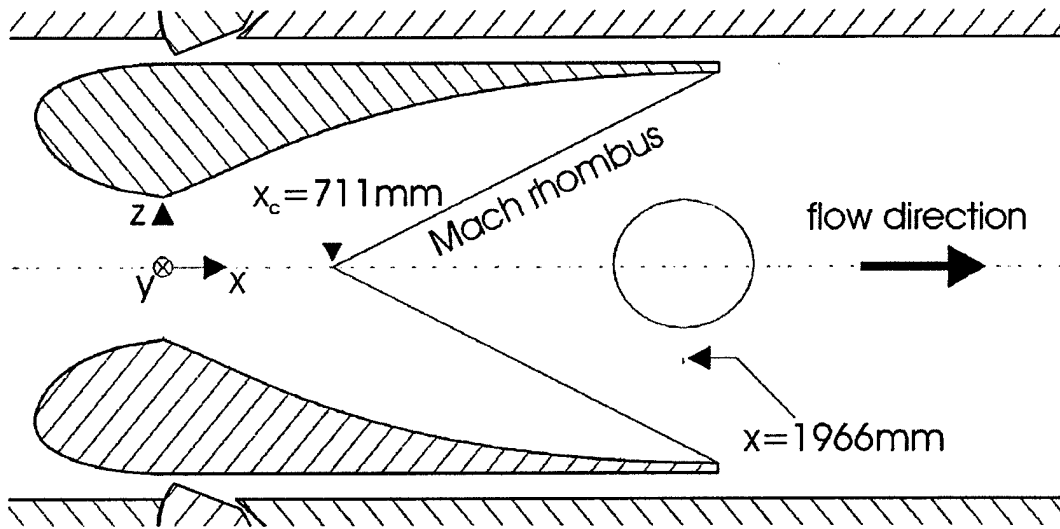


Figure 7: Test section of SWK.

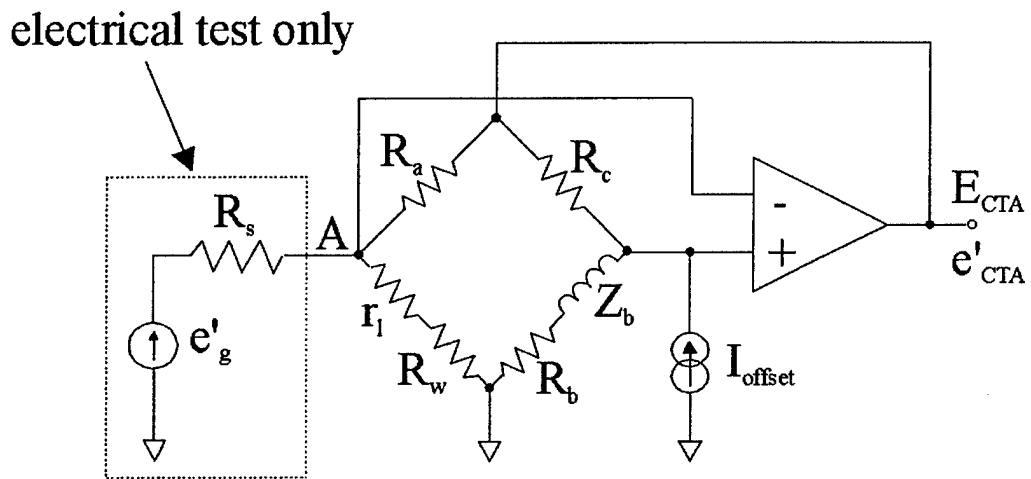


Figure 8: CTA circuit.

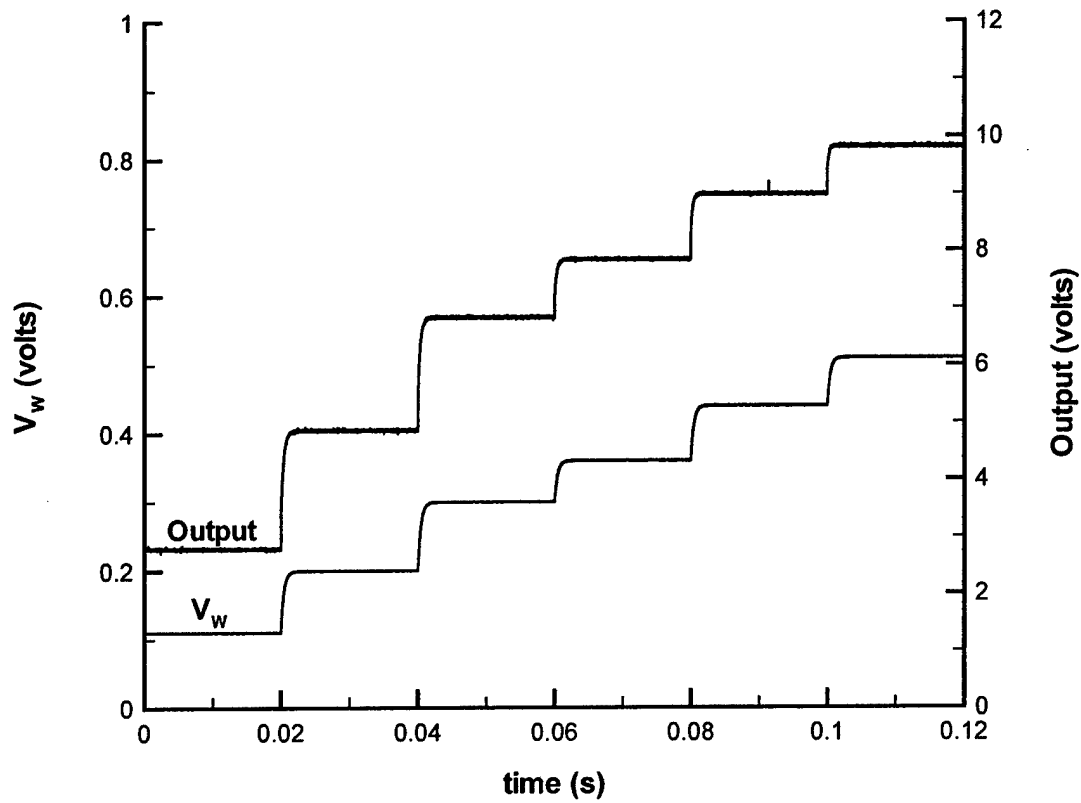
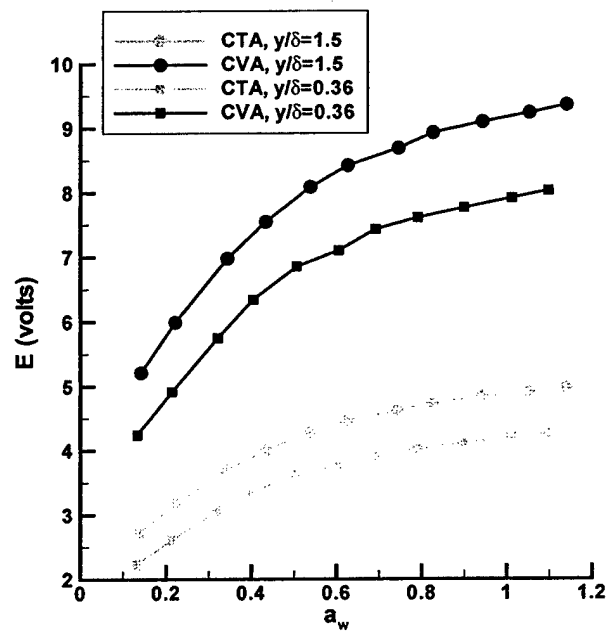


Figure 9: Automatic stepping of the hot-wire voltage for CVA.



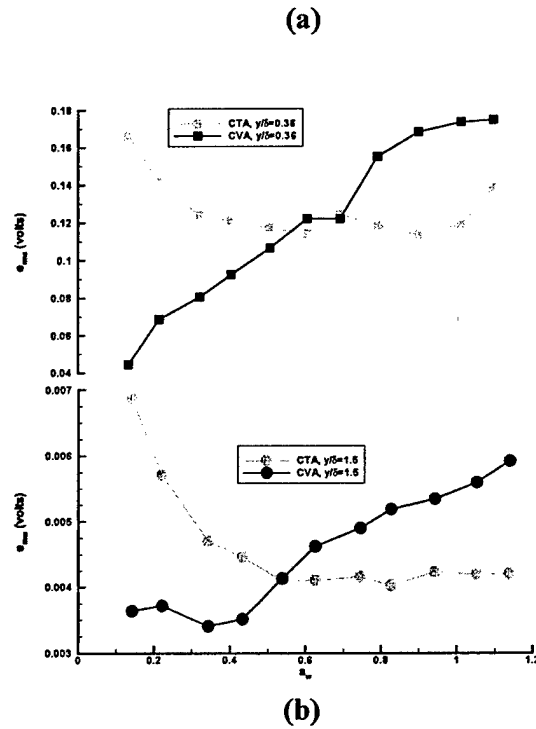


Figure 10: Anemometer mean and rms output voltages (a) Mean. (b) rms.

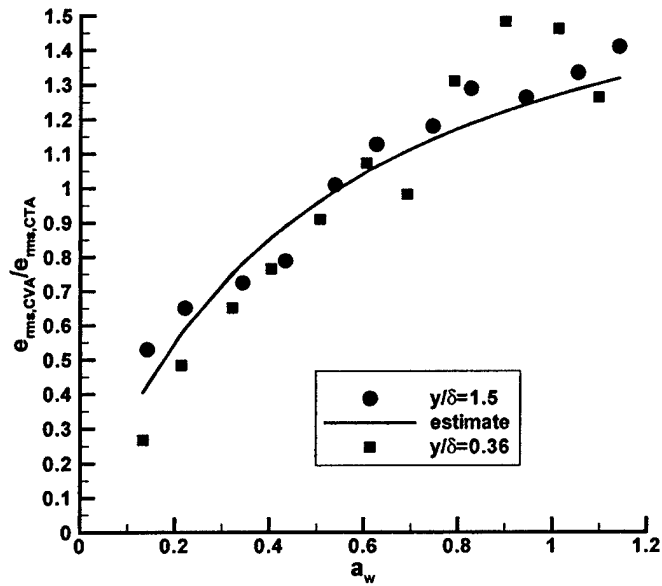


Figure 11: Estimated ratio of anemometer rms output voltages.

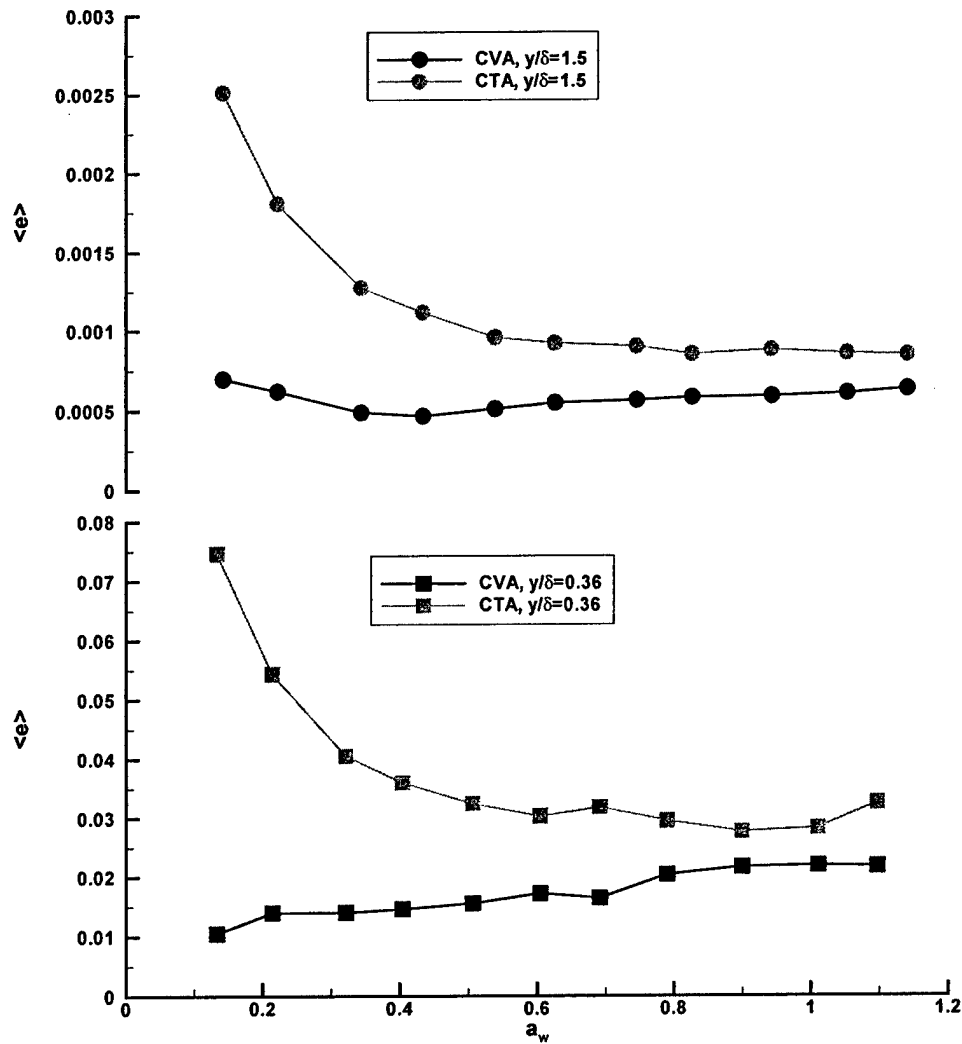
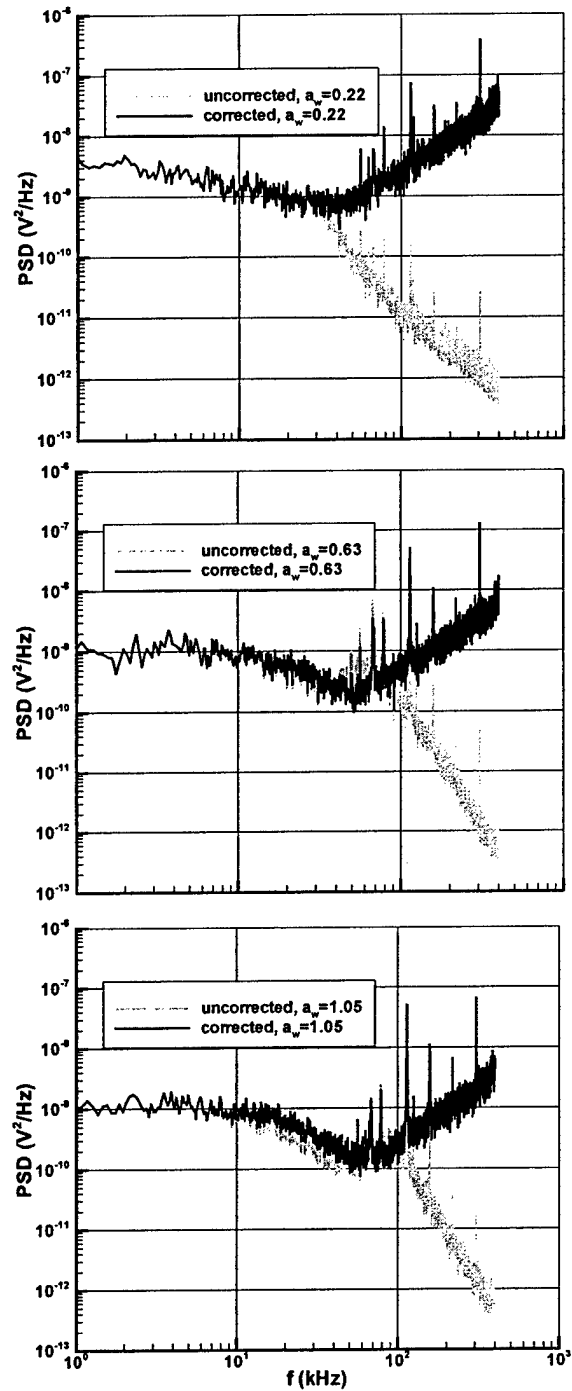


Figure 12: Normalized anemometer output voltages.



**Figure 13: Software corrected and uncorrected CTA spectra measured in freestream.**

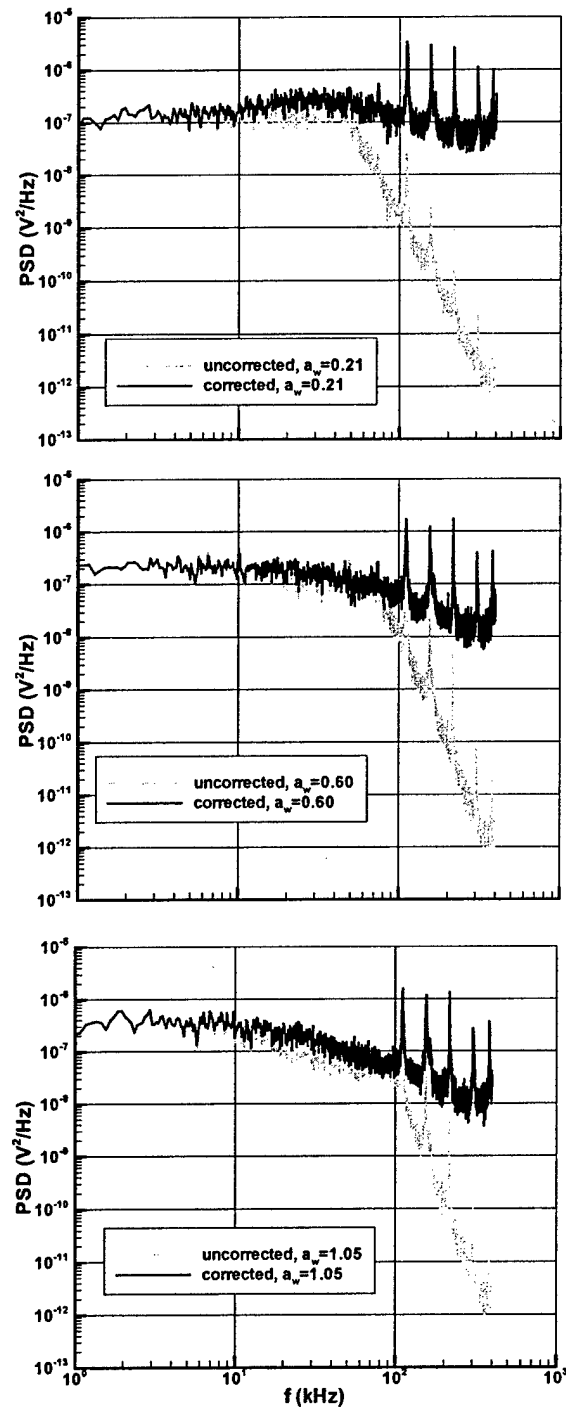


Figure 14: Software corrected and uncorrected CTA spectra measured in boundary layer.

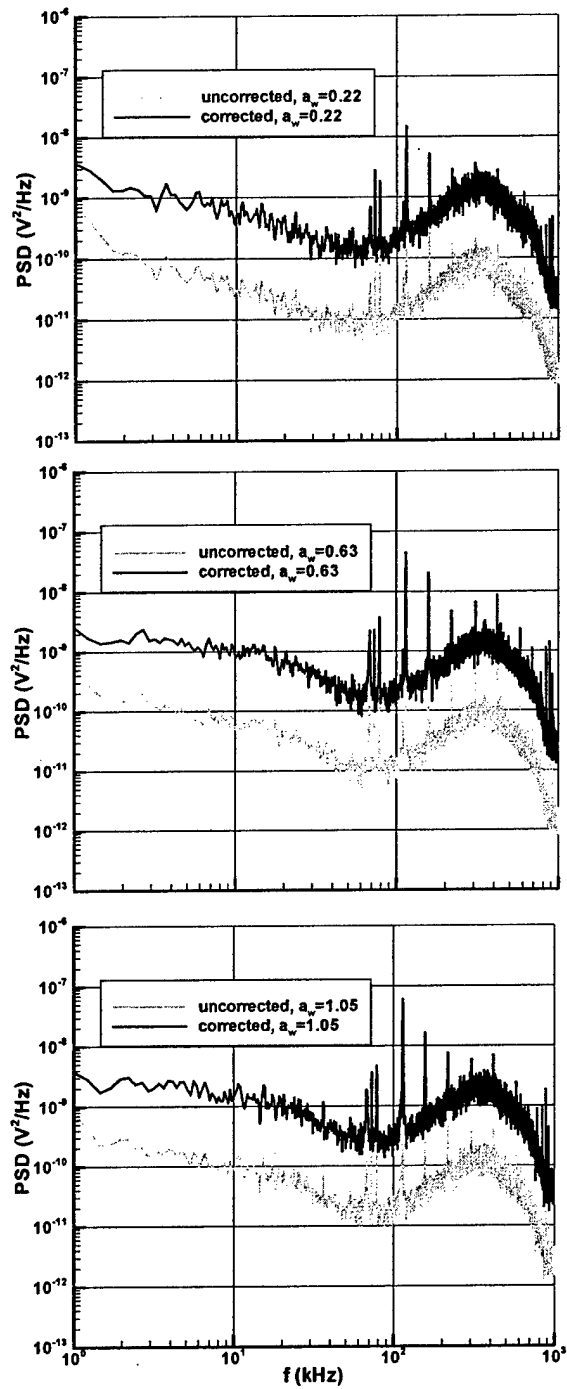


Figure 15: Software corrected and uncorrected CVA spectra measured in freestream.

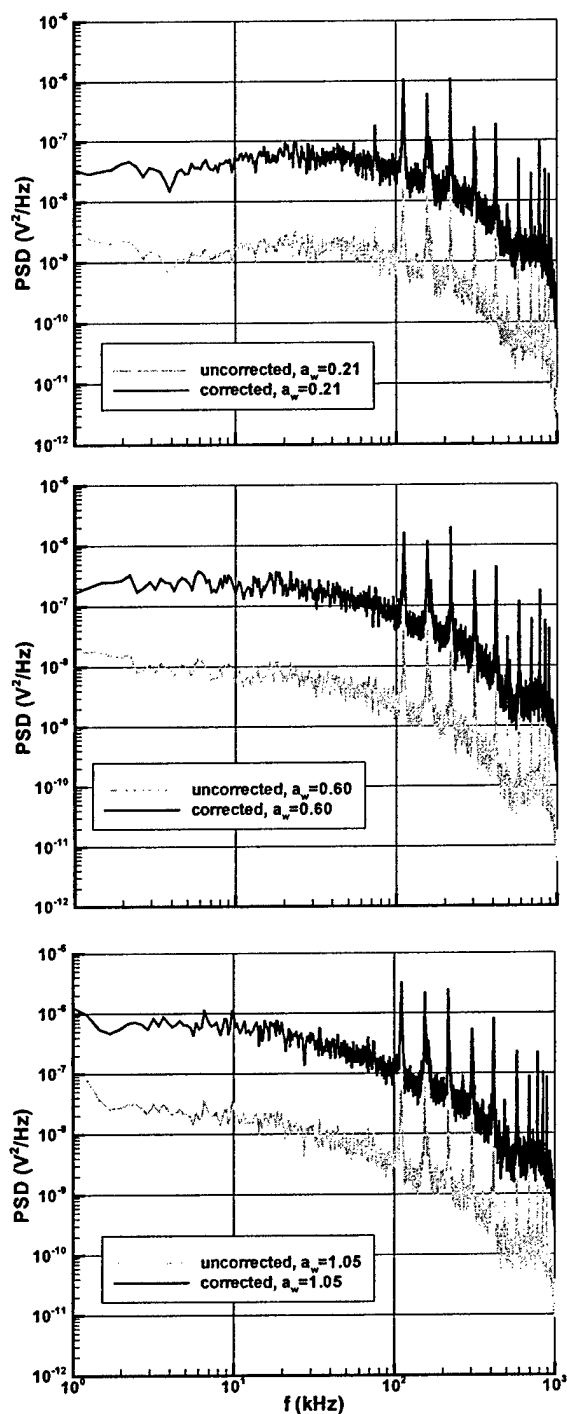


Figure 16: Software corrected and uncorrected CVA spectra measured in boundary layer.

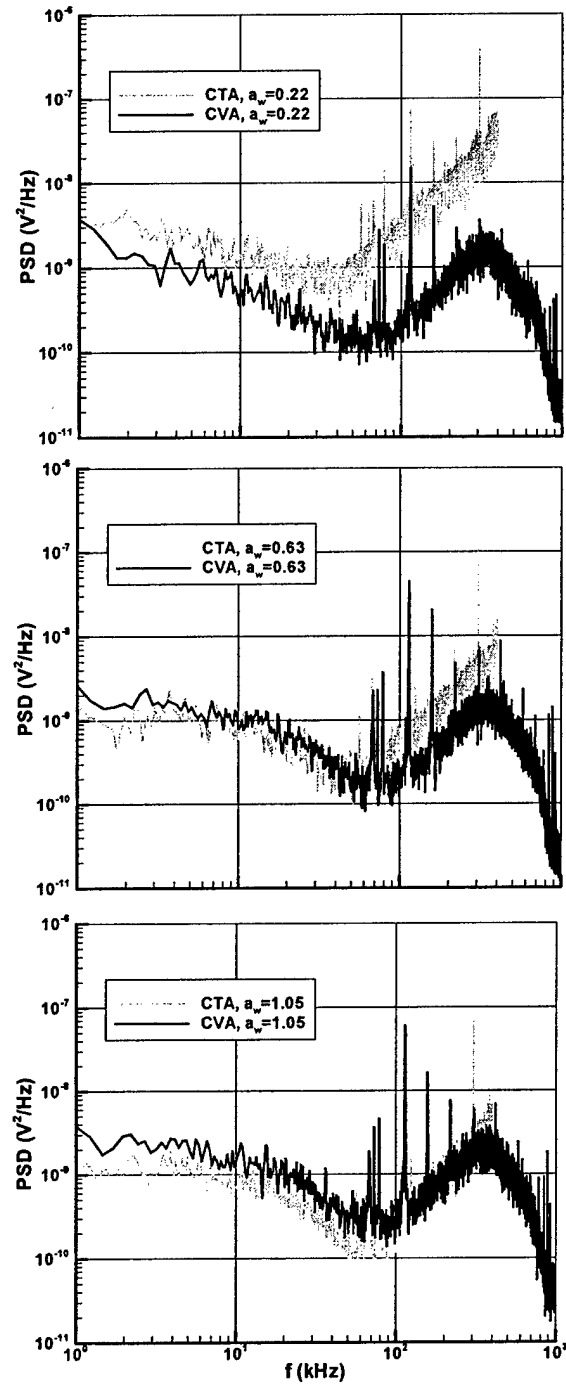


Figure 17: Comparison of corrected CTA and CVA spectra measured in freestream.

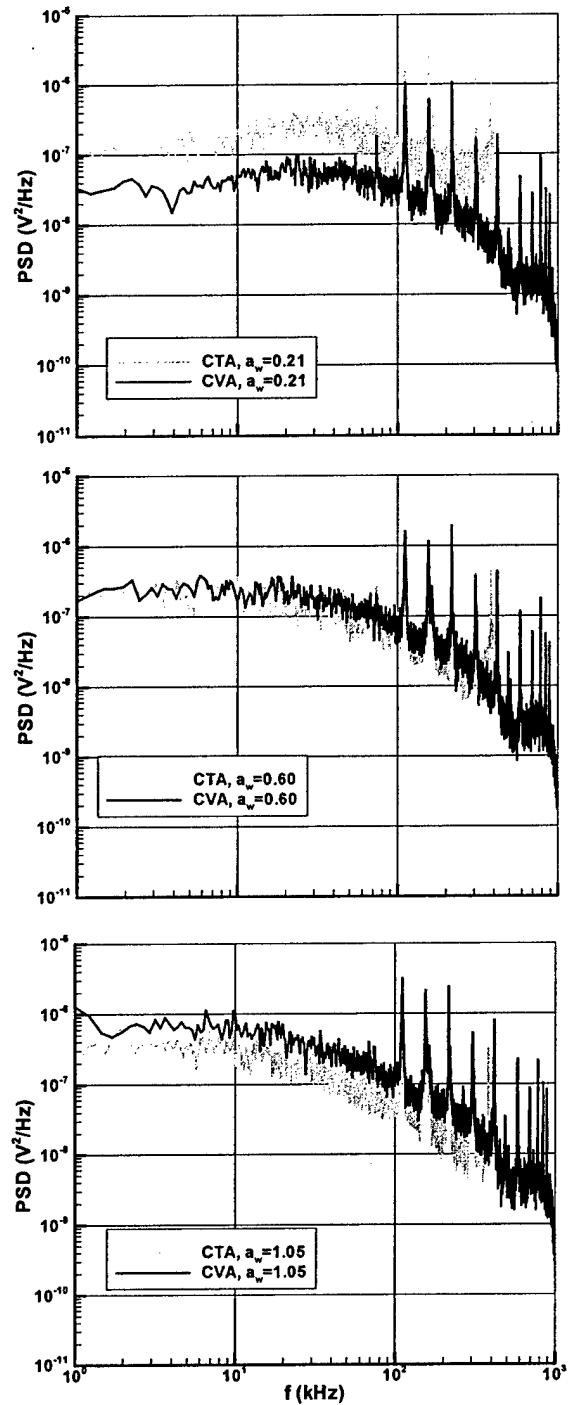


Figure 18: Comparison of corrected CTA and CVA spectra measured in boundary layer.

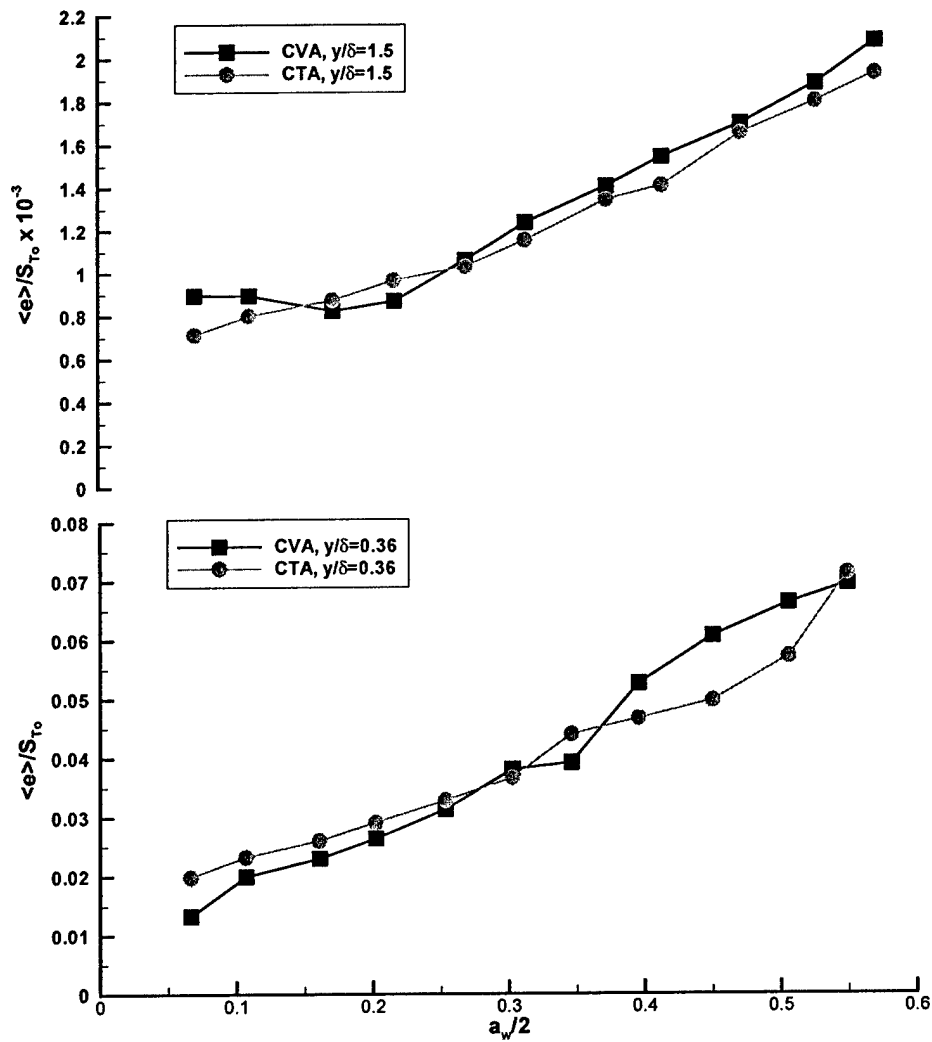


Figure 19: Fluctuation diagrams.

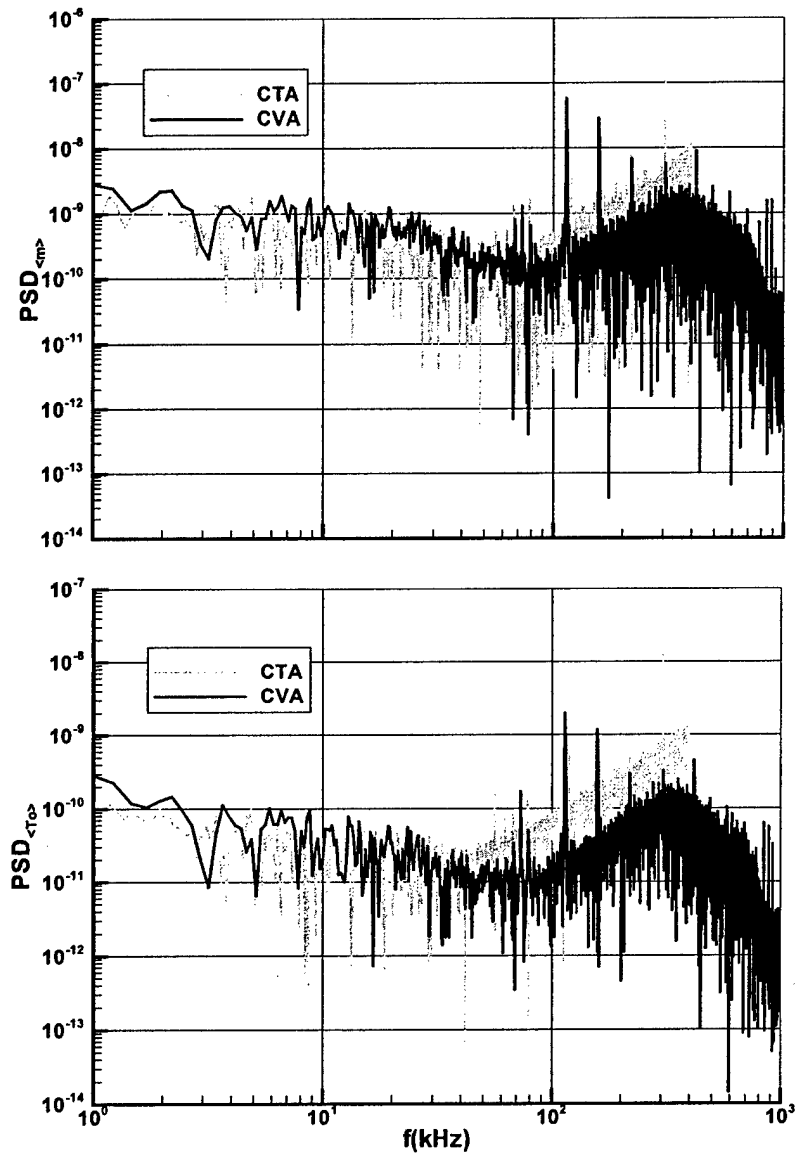


Figure 20: Comparison of mass flux and total temperature spectra measured in freestream.

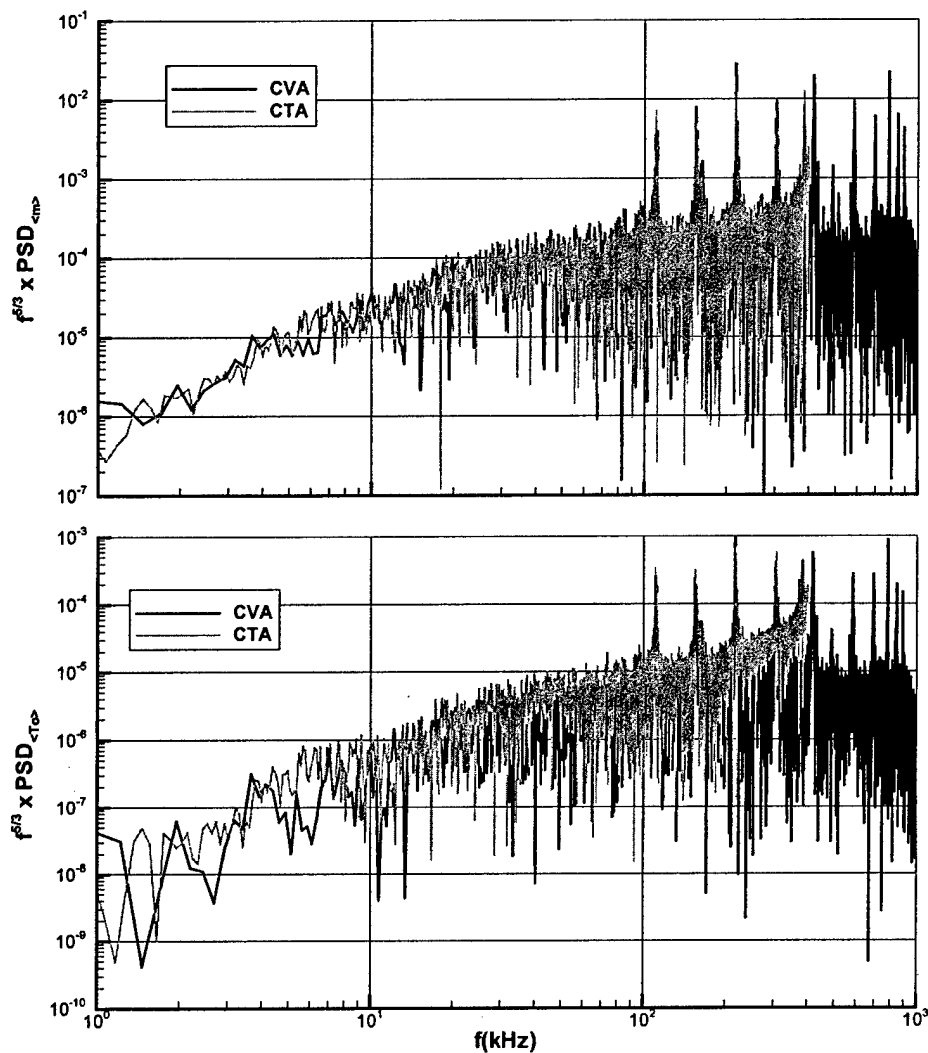


Figure 21: Comparison of mass flux and total temperature spectra measured in boundary layer.



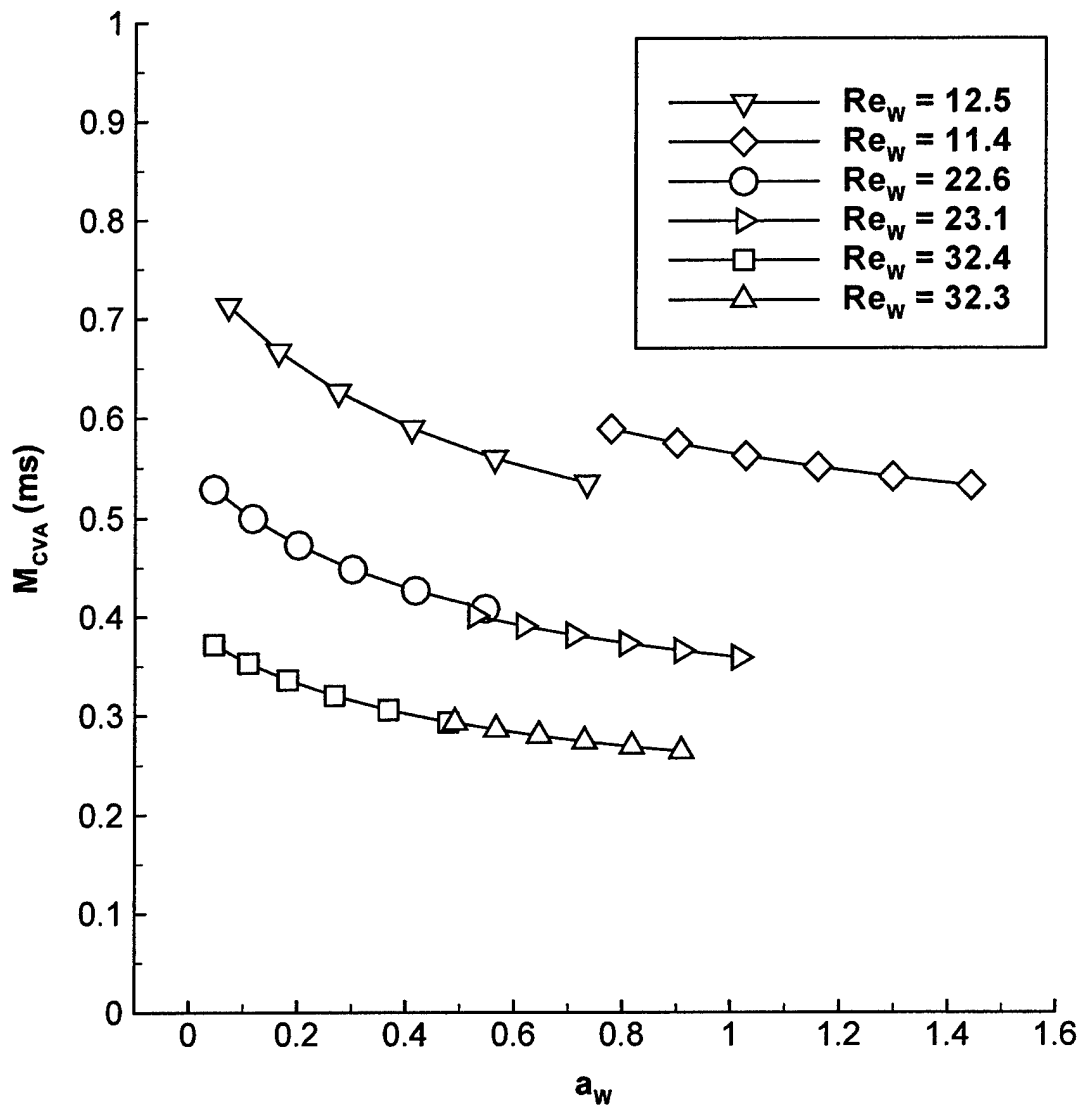


Figure 22: Estimated hot-wire time constant for SWK.

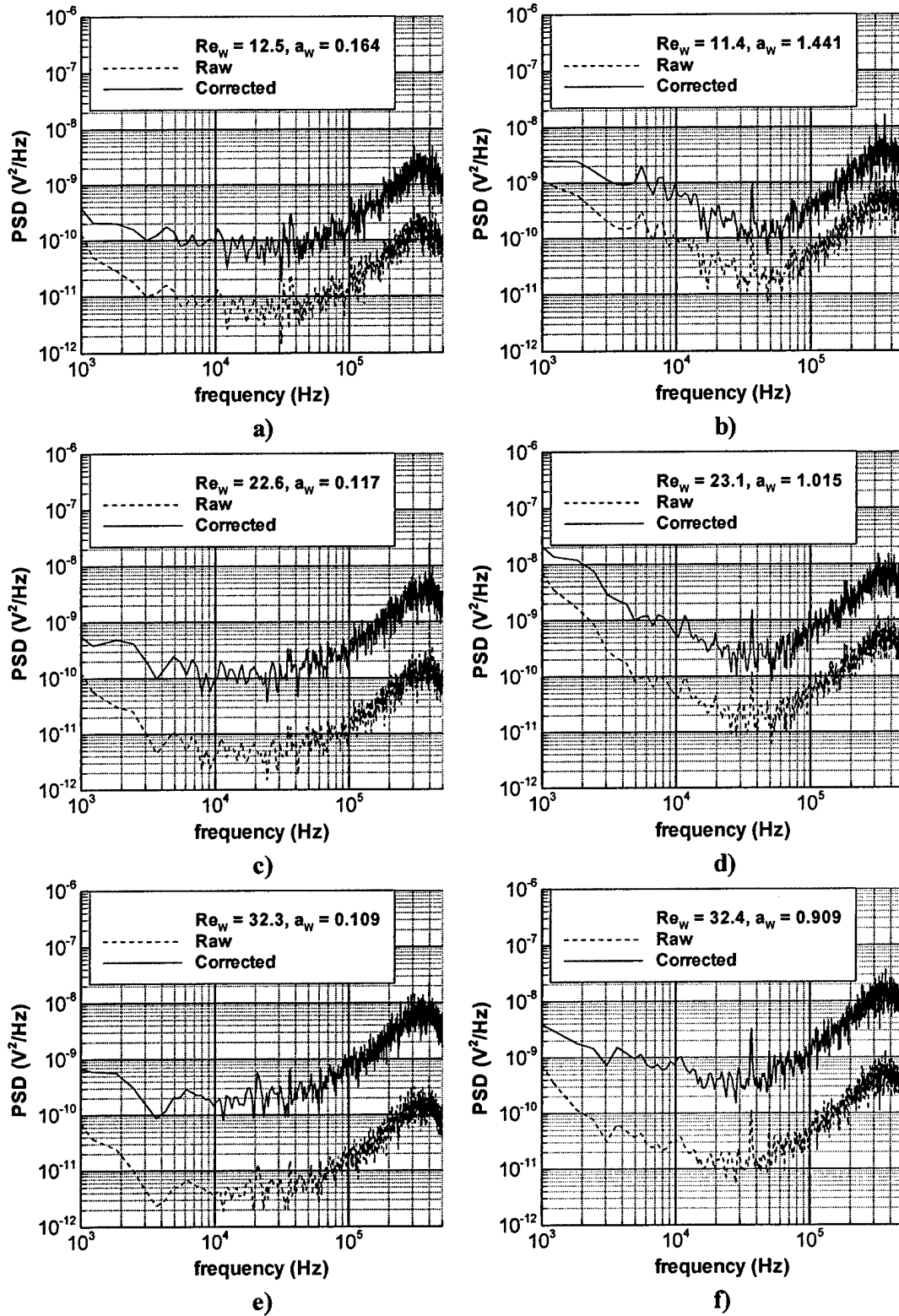
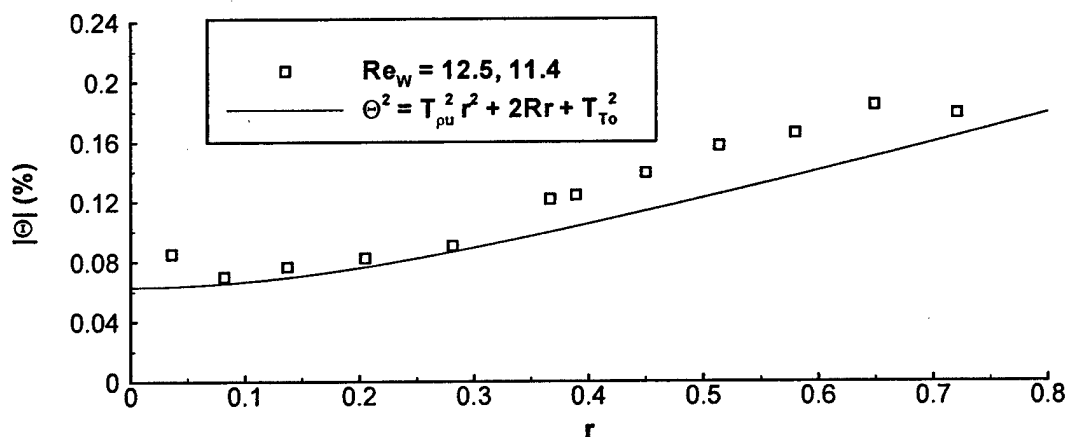


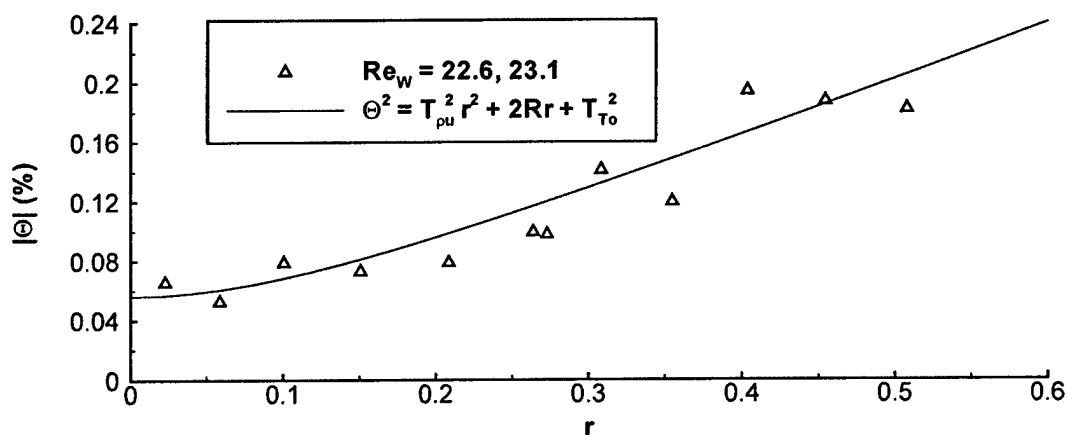
Figure 23: Spectra of hot-wire measurements in the SWK freestream.

*Calibration and Optimization of Constant Voltage Hot-Wire Anemometer in Hypersonic Flows*

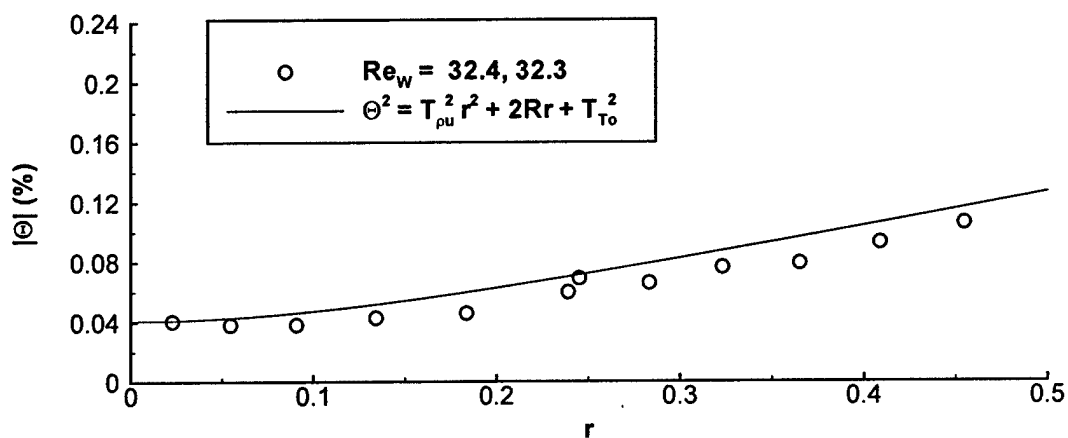




a)



b)



c)

Figure 24: Fluctuation diagrams for the SWK.